Photo/Redox-Responsive 2D-Supramolecular Assembly Involving Cucurbit[8]uril and a Star-Shaped Porphyrin Tecton

Shagor Chowdhury, Youssef Nassar, Laure Guy, Denis Frath, Floris Chevallier, Elise Dumont, Ana Paula Ramos, Grégoire Jean-François Demets, Christophe Bucher

Photo/Redox-Responsive 2D-Supramolecular Assembly Involving Cucurbit[8]uril and a Star-Shaped Porphyrin Tecton

Shagor Chowdhury[§], Youssef Nassar[§], Laure Guy[§], Denis Frath[§], Floris Chevallier[§], Elise Dumont[§], Ana Paula Ramos[¥], Grégoire Jean-François Demets[¥*], Christophe Bucher[§*]

[§]*Univ Lyon, Ens de Lyon, CNRS UMR 5182, Université Claude Bernard Lyon 1, Laboratoire de Chimie, F69342, Lyon, France.* christophe.bucher@ens-lyon.fr

[¥]*DQ-FFCLRP, Universidade de São Paulo. Av. Bandeirantes 3900, CEP 14040-901, RibeirãoPreto S.P. Brazil. (55) 16 3315 4860. greg@usp.br*

Abstract

The present paper reports on the formation and on the electrochemical/spectroscopic characterization of inclusion complexes formed in aqueous media between cucurbit[7 or 8]urils cavitands (CB[7], CB[8]) and a rigid four-pointed star-shaped viologen-appended porphyrin tecton. The formation of discrete 4:1 pseudo-rotaxane-like caviplexes, involving threading of CB[n] rings on the rigid viologen-based star's branches has been demonstrated by nuclear magnetic resonance and mass spectrometry measurements. Then, the photo- and redox-triggered formation of 2D supramolecular assemblies involving CB[8]s and the four electron reduced tectons as key building elements, has been established on the ground of in-depth electrochemical and spectroscopic analyses supported by quantum calculations. The CB[8]-promoted intermolecular π-dimerization of the viologen cation radicals introduced at the *meso* positions of the porphyrin plateform has been brought to light through the diagnostic signatures of the 1:2 host-guest ternary caviplexes formed between viologen and CB[8] and by spectroscopic data collected after electrochemical, chemical or photochemical reduction of the viologen-based tectons. The CB[8] hosts not only proved useful to promote the redox-triggered formation of supramolecular assemblies, it was also found to prevent the chemical reduction of the porphyrin ring in aqueous media and its subsequent conversion into phlorin products.

keywords: π-dimer, Responsive Supramolecular Assembly, Viologen Cation Radicals, Cucurbituril, Porphyrin, Phlorin.

Introduction

Self-assembly spontaneously occurs between molecules capable of interacting with one another through non-covalent interactions. Nature offers a whole range of biologically relevant supramolecules, like DNA wherein simple molecular building blocks are organized into functional structures *via* a complex network of orthogonal, non-covalent bonds. The efficiency of the assembling process, the dimensionality, strength and organization of the network can more or less be estimated from the number and directionality of the "weak" interactions involved, as well as on the geometrical features of the elementary unit carrying the assembly code, also known as a tecton [1-4]. The large palette of interaction concealed in the supramolecular toolbox, varying in directionality and strength, from the weakest Van der Waals dispersion forces to highly directional hydrogen bonds and strong electrostatic interactions, have already demonstrated their great potential for promoting the assembly of carefully designed molecular tectons into 1D wires, 2D surfaces or 3D networks. The reversible and dynamic nature of the "interactions" involved in such assemblies has moreover opened up exciting opportunities for the development of stimuli-responsive materials, for instance to achieve a control over the association/organization between tectons with an external stimulus (Figure 1A) [5-9].

Our group has been focusing over the past few years on the development of tailor-made redox-controllable molecular or supramolecular systems involving electrogenerated viologen-based π-cation radicals $R_1\mathbf{V}R_2^{+\bullet}$ in Figure 1B) as key responsive and/or assembling elements, using their ability to self-assemble into sandwhich-like, dimeric entities called π-dimers ($[(R_1VR_2)_2]^{2+}_{dim}$ in Figure 1B) [10-20]. These studies, and many others [16, 21-29], have served to establish that the effective formation of such multi-center bonded dimers in solution actually requires either very low temperatures and/or high concentrations in radicals. As an alternative, viologen-based π-dimers can also be observed in standard temperature and concentration ranges, when using barrel–shaped cavitan ds known as cucurbit[8]urils (CB[8]), made of 8 glycoluril moieties connected by methylene bridges, whose inner cavity is ideally suited to the inclusion of two viologen-based radicals [30-35]. Such process is illustrated in Figure 1C with a calculated structure of the inclusion complex $[(R_1\mathbf{V}R_2)_2]^{2+}_{dim} \subset$ CB[8] obtained upon mixing CB[8] with two equivalents of *N,N′*-dimethyl-4,4′-bipyridinium radicals $R_1\mathbf{V}R_2^{2+}$.

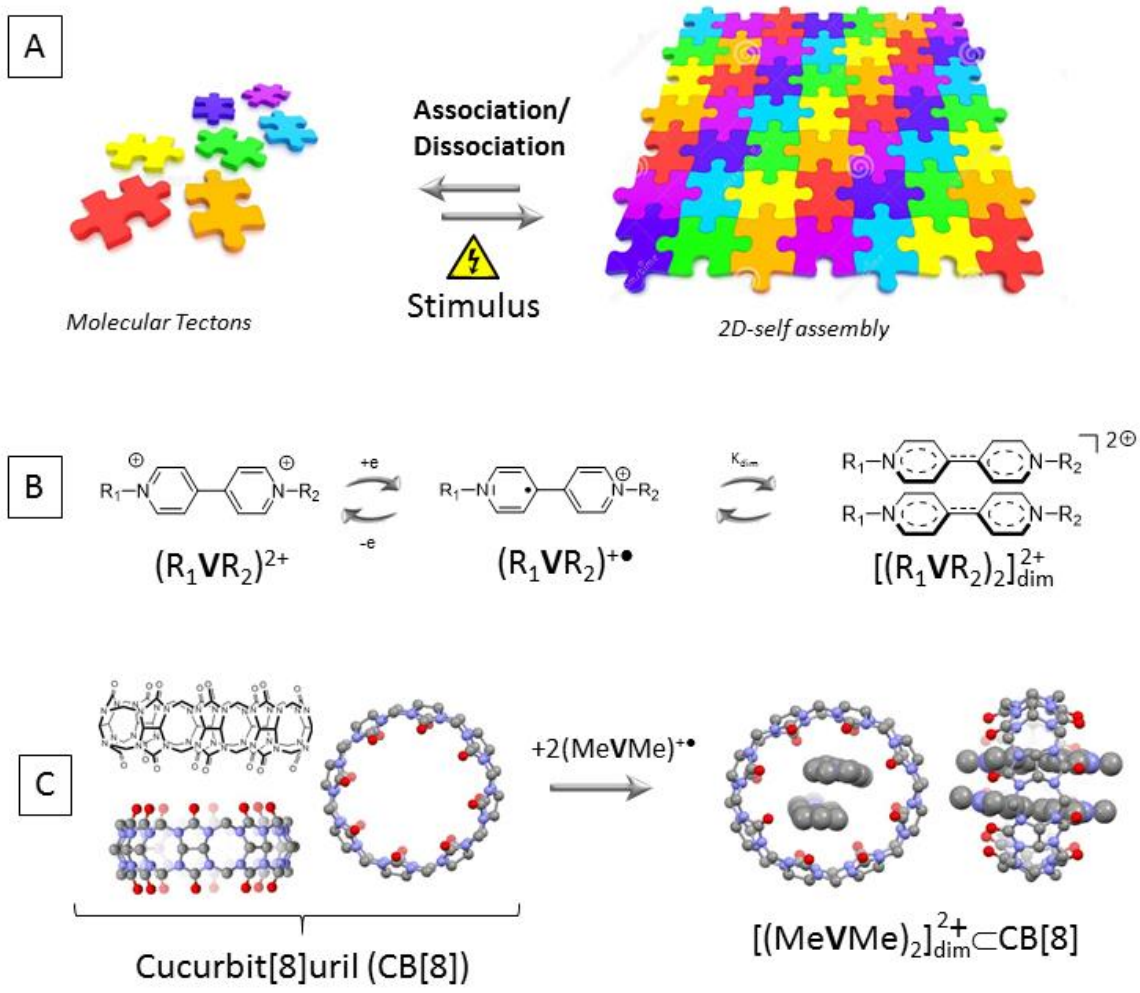

Figure 1. Schematic representation of A) a stimuli-responsive 2D-self-assembly process, B) the electron-triggered π-dimerization of two viologen-based cation radicals. C) the calculated structure (DFT level) of the barrel-shaped host CB[8] and of the inclusion complex $[(R_1\mathbf{V}R_2)_2]^{2+}_{dim} \subset$ CB[8].

As a matter of facts, the high affinity of CB[n]s (n = 7 or 8) for viologens dications and cation radicals has been extensively used over the past decades to devise a wide range of redox- or chemically-responsive rotaxane-like molecular systems [36, 37]. More recently, viologen and cucurbiturils have also been considered as key building blocks in the development of various potentially responsive 2D/3D self-assembled structures [30, 35, 38, 39], the underlying idea being that the dimensionality of the assemblies can be tuned with the number of viologens units available on each tectons.

In the present article, we are reporting on our approach towards redox-responsive self-assembled systems involving cucurbiturils hosts and a tetratopic, four-pointed star-shaped viologen appended porphyrin as building elements (**1**M^{8+} in Figure 2). It includes spectroscopic analyses of the host-guest processes occurring between **1**M^{8+} and CB[7] or CB[8] in aqueous

media as well as detailed electrochemical investigations carried out in organic and aqueous media to assess the ability of the CB[8] host to promote the intermolecular π-dimerization of the four–electron reduced species **1**$M^{(4+\bullet)}$.

Synthesis

The multi-step synthesis of the key tetratopic tecton, namely the tetra(*meso*-viologen)porphyrins **1**M^{8+} (M = H_2 or Zn), is summarized in Figure 2. This synthesis is actually the result of an improvement of a previously reported procedure [40]. The starting point is a standard Rothemund condensation of pyrrole with 4-nitrobenzaldehyde in a propionic acid/acetic anhydride mixture yielding the corresponding 5,10,15,20-tetrakis(4'-nitrophenyl)porphyrin **4**H_2 in 30% yield. Reduction of the nitro group, carried out in an acidic medium in the presence of $SnCl_2.2H_2O$, led with quite good yield to the 5,10,15,20-tetrakis(4'-aminophenyl)porphyrin intermediate **2**H_2, obtained as a dark-blue crystals. The latter compound was then metalated with an excess of zinc (II) acetate at room temperature to afford **3**Zn in a quantitative yield. The targeted compounds **1**H_2^{8+} and **1**Zn^{8+} have *in fine* been obtained through multiple Zincke coupling reactions [41] involving the activated Zincke salt $\mathbf{2}^{2+}$ as reactant [42]. The real bottleneck of this ultimate step was the purification process which was successfully achieved by column chromatography using a mixture of ACN:H_2O:KNO_3 (12:7:7) as eluent.

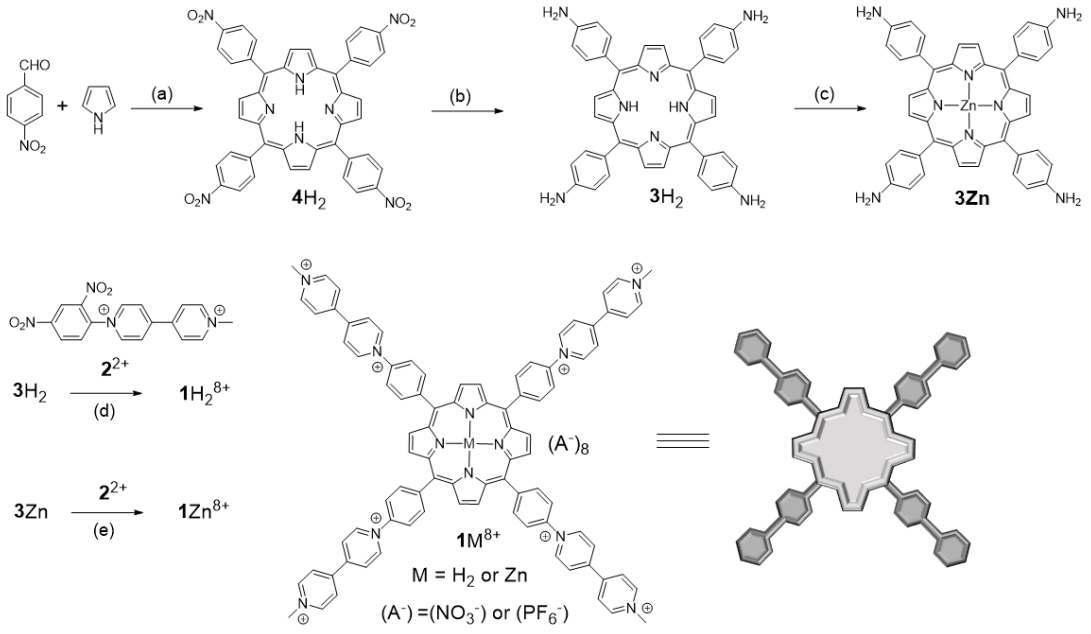

Figure 2. Elaboration of the tetrakis(methyl-phenyl-viologen)porphyrins. (a) $EtCO_2H$, Ac_2O, reflux, 4 h, 30%; (b) $SnCl_2{\cdot}2H_2O$, conc. aq. HCl, reflux, 16 h, 62%; (c) $Zn(OAc)_2$, DMF, 25 °C, 30 min, >99%; (d) $2(PF_6)_2$, EtOH, H_2O, reflux, 18 h, 29%; (e) $2(PF_6)_2$, EtOH, H_2O, reflux, 18 h, 32%.

Threading of the CB[7] or CB[8] rings on 1M^{8+}

As mentioned in the introduction, both the CB[7] and CB[8] hosts have the ability to form [1:1] inclusion complexes with dicationic viologen-based guests (R_1**V**R_2^{2+} in Figure 1B). Our primary objective was thus to get accurate and reliable information on the binding mode (stoichiometry, structure) between our star-shaped guest and those barrel-shaped hosts. As a first step, the interactions of **1**Zn^{8+} with CB[7] and CB[8] have been investigated in deuterated water by NMR spectroscopy. The exact attribution of all the NMR signals discussed below has been achieved through careful analysis of 1D- spectra and 2D correlation maps provided in the ESI section (see Figure ESI 1-8).

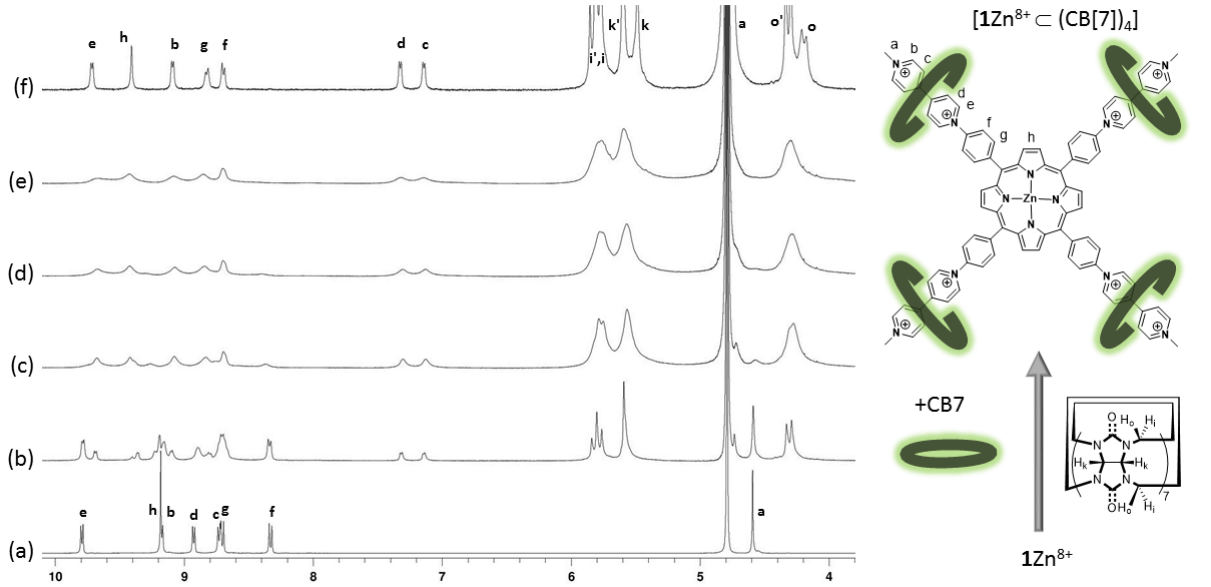

Figure 3. ^{1}H NMR spectra (400 MHz, D_2O) of 1Zn$(NO_3)_8$ (a) at 1.0 mM in the absence and in the presence of (b) 1.0 equiv. of CB[7] at 1.0 mM, (c) 2.0 equiv. of CB[7] at 1.0 mM, (d) 4.0 equiv. of CB[7] at 1.0 mM, (e) 8.0 equiv. of CB[7] at 1.0 mM, (f) 8.0 equiv. of CB[7] at 0.1 mM.

The changes observed in D_2O upon addition of increasing amounts of CB[7] are shown in Figure 3. In the absence of cucurbituril, the spectrum of **1**Zn^{8+}exhibits 6 doublets at low field attributed to the hydrogen atoms located on the viologen (b,c,d,e) and phenyl (f,g) units, as well as two singlets attributed to the hydrogens of the porphyrin and N^+-Me moieties. It is worth noting that the most and least shielded (hetero)aryl signals, resonating at about 9.8 and 8.35 ppm, are attributed to the hydrogen atoms located on the adjacent pyridinium and phenyl rings, respectively (e and f in Figure 3). As can be seen in Figure 3, the host-guest equilibria involved in solution upon addition of CB[7] are kinetically slow at the NMR time scale. The targeted threading process, involving inclusion of the viologen axles into the CB7 rings, is indeed clearly

revealed by the gradual disappearance of all the signal attributed to the free **1**Zn^{8+} guest at the expense of new sets of signals attributed to different inclusion complexes, incorporating either 1, 2, 3 or 4 CB[7] hosts, noted [**1**$Zn^{8+} \subset$ **(**$CB[7])_n$] (with $1 \leq n \leq 4$). An in-depth analysis of the data depicted in Figure 3 provided further insights into the stoichiometry of the complexation (determination of n) and into the structure of the host-guest complexes (relative position of the CB rings on the viologen-based axle). The maximum number of CB hosts that can be threaded onto the viologen-appended porphyrin platform could indeed be readily inferred from this titration experiment reaching completion after addition of four molar equivalents of CB, which is in agreement with the complexation of one viologen per CB to yield the inclusion complex [**1**$Zn^{8+} \subset$ **(**$CB[7])_4$] (see right-hand side drawings in Figure 3). Then, the upfield shift of more than 1.6 ppm experienced by the inner hydrogens of the viologen units (H_c, H_d), taken together with the limited shift of about 0.1-0.2 ppm of the outer ones (H_b, H_e), supports the conclusion that the CB[7] rings lie between both pyridinium rings. The macrocyclic host is in part stabilized at this exact location with a network of hydrogen bonds linking the outer oxygen atoms of the CB host and the terminal hydrogen atoms of the N^+-methyl substituents, as revealed by the downfield shift of about 0.2 ppm experienced by the singlet attributed to H_a.

The inclusion of the viologen units has also a significant impact on the chemical shift of the signals attributed to the CB hosts. In the absence of guest, CB[7] displays one singlet at 5.53 ppm attributed to H_k and two doublets at 4.23 and 5.80 ppm, attributed to the hydrogens of the methylenic bridge pointing outside (H_o) or inside (H_i) the cavity of CB[7], respectively.[43] As can be seen in the early stage of the titration (Figure 3), the threading of a non-symmetrical viologen-based axle through CB[7] also results in the splitting of the H_i protons, observed as two partially overlapped doublets (pseudo triplet at 5.80 ppm) in the spectrum of the inclusion complex. The effect of the viologen-based guests on the CB[7] hosts is further revealed on the spectrum recorded at low concentration of **1**Zn^{8+} (0.1 mM) in the presence of 8 equivalents of CB[7] (top spectrum in Figure 3) through the observation of different sets of signals corresponding to the free (i',o',k') and complexed (i,o,k) CB[7]s.

A similar investigation has been carried out with the less soluble CB[8] host, featuring a wider inner cavity but still capable of forming 1/1 inclusion complexes with viologens derivatives [34, 44, 45]. The stoichiometry and structure of the assembly is also deduced from the titration data depicted in **Figure 4**. As observed with CB[7], the largest chemical shifts involve H_c and H_d and the titration reached completion after addition of 4 molar equivalents of CB[8]. These results thus support the conclusion that four CB[8] rings can be threaded onto **1**Zn^{8+} and that the macrocyclic guest lies in between both pyridinium rings. The impact of binding on the

chemical shift of the host is also found to be less pronounced for CB[8] than for CB[7]. This size effect is for instance revealed in the spectra of [**1**Zn^{8+} ⊂ **(**CB[7])$_4$] and [**1**Zn^{8+} ⊂ **(**CB[8])$_4$] through the observation of Hi as a broad singlet for CB[8] and as two singlets for CB[7].

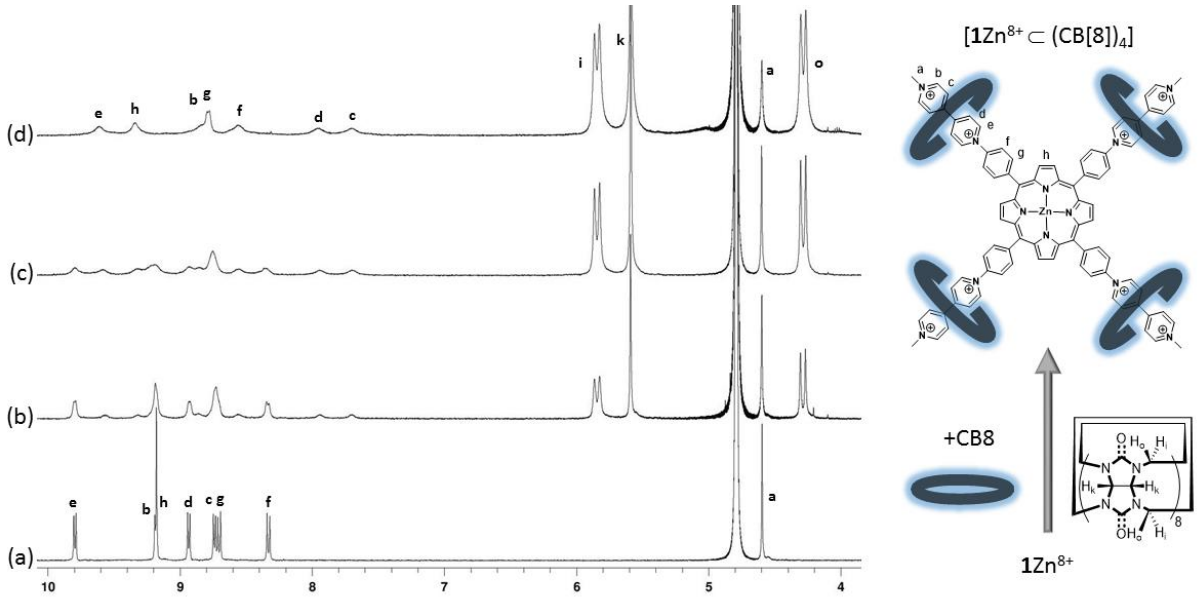

Figure 4. ^{1}H NMR spectra (400 MHz, D_2O, 0.1 mM, 293 K) of $1Zn(NO_3)_8$ (a) in the absence and in the presence of (b) 1.0 equiv. of CB[7], (c) 2.0 equiv. of CB[7], (d) 4.0 equiv. of CB[7].

After equilibration, the self-assembled host-guest complex [**1**Zn^{8+} ⊂ **(**CB[7])$_4$] has been further characterized by electrospray ionization mass spectrometry. The spectrum obtained with a Q-TOF instrument equipped with an electrospray ionization source in the presence of a formate buffer showed [**1**Zn(CB[7])$_4$,(HCO_2)]$^{7+}$ as the base peak at m/z=865. The spectrum shown in **Figure 5** also include a range of less intense signals attributed to the [**1**Zn(CB[7])$_4$,$(HCO_2)_2$]$^{6+}$ (m/z 1016.6) and [**1**Zn(CB[7])$_4$]$^{8+}$ (m/z 751.2) ions.

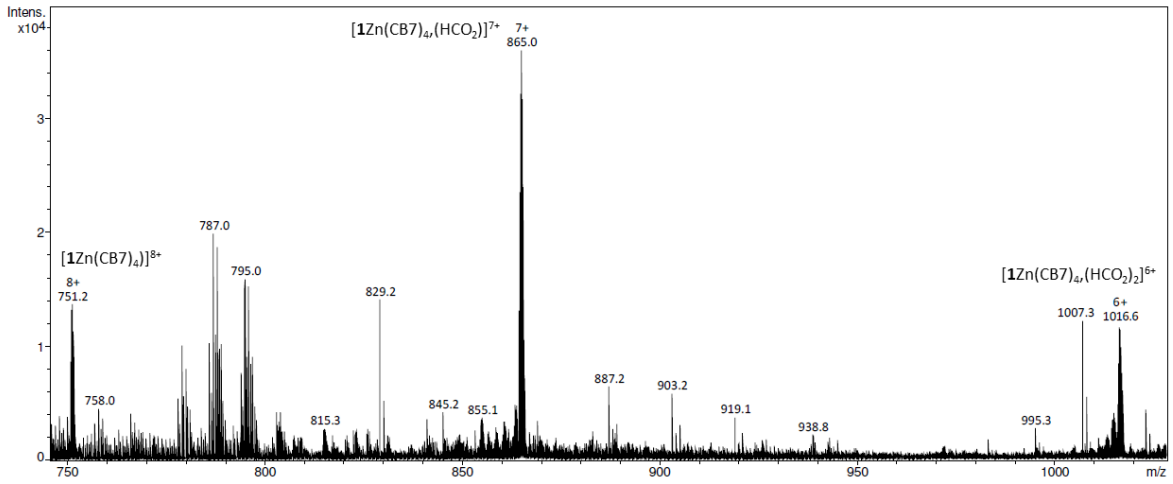

Figure 5. Positive electrospray spectrum of the $[1Zn^{8+} \subset (CB[7])_4]$ assembly.

Taken all together, the NMR and MS data discussed above support the effective inclusion of the four viologen units available on the porphyrin platform in the cavity of CB[7] or CB[8] to yield the caviplex compounds $[\mathbf{1}Zn^{8+} \subset (CB[n])_4]$. The feasibility of such association, and most specifically the absence of steric hindrance between the CB and porphyrins units and between the neighboring CB units was checked by computational analyses carried out on the fully complexed $[\mathbf{1}Zn^{8+} \subset (CB[8])_4]$ compound. The minimized structure obtained at the DFT level is depicted in a dedicated section at the end of the article (**Figure 16**). The latter reveals the absence of steric clashes of any sort, neither between the threaded macrocycles nor between the porphyrin skeleton and the CBs.

Following these initial findings, we focused on the association between the CB hosts and the electrogenerated four-electron reduced species $\mathbf{1}M^{4(+\bullet)}$

Electrochemistry in organic medium

The electrochemical signatures of the title compounds $\mathbf{1}H_2(PF_6)_8$ and $\mathbf{1}Zn(PF_6)_8$ have first been investigated in DMF using *n*-tetrabutylammonium perchlorate (TBAP) as the electrolyte. Both compounds display similar signatures featuring four consecutive reductions (noted E^{1c}, E^{2c}, E^{3c} and E^{4c} in Table 1) and one oxidation (noted E^{1a}) in the accessible potential window (Figure 6). The first reversible wave centered at $(E_{1/2})^{1c}$ =–0.762 mV is attributed to the one electron reduction of the four viologens units (one electron per viologen) in $\mathbf{1}Zn^{8+}$ yielding the tetra-cationic compound $\mathbf{1}Zn^{4(+\bullet)}$. The shape of this wave, featuring a standard ΔE_P value of about

63 mV reveals the absence of "communication" between each viologens introduced at the *meso*-positions of the π-conjugated porphyrin ring. Savéant has established in the early seventies that electron transfers to or from molecules containing n identical, non-interacting, redox centers should yield simple CV curves similar to that observed with a single electroactive center (ΔE_P ~ 58 mV at 25°C) but with current values determined by the total number of redox centers [46, 47]. When each center is characterized by the same formal potential and adheres to the Nernst equation independently of the oxidation state of any of the other centers in the molecule, it is possible to calculate the formal potentials corresponding to each pair of n successive oxidation states of the molecules. Considering fully non-interacting centers, the theoretical shift between the first viologen-based formal reduction potentials in **1**Zn^{8+} ($E^{0'}_{1\_1}$, $E^{0'}_{1\_2}$, $E^{0'}_{1\_3}$, $E^{0'}_{1\_4}$ in Figure 6) should thus equal $\Delta E^0_1 = E^0_{1\_n} - E^0_{1\_(n-1)}$ = 23.7 mV, although the overall four electron reduction appear *in fine* as a single reversible wave with peak potentials satisfying ΔE_p ~ 60 mV.

The second one electron reduction of the viologen units (one electron per viologen) is observed at $(E_{1/2})^{2c}$ = -1,087 V as a reversible wave. Here again, there is no experimental evidence supporting the existence of intramolecular "interactions" between the redox centers and the same comments on the four electron reduction **1**$Zn^{8+} \rightarrow$ **1**$Zn^{(4+\bullet)}$ apply for **1**$Zn^{(4+\bullet)} \rightarrow$ **1**Zn. It is worth mentioning here that the stability domain measured for the viologen cation state in **1**$Zn^{(4+\bullet)}$ [$\Delta E = (E_{1/2})^{2c} - (E_{1/2})^{1c}$ = 325 mV], falling within the range of that measured in the same conditions with the simple dimethyl viologen Me**V**Me^{2+} (ΔE = 336 mV, see Table 1) used as a reference, is a first evidence suggesting the absence of intermolecular interactions between the viologen cation radicals in solution [16].

The porphyrin ring is also submitted to two consecutive one-electron reduction at $(E_{1/2})^{3c}$ = −1.827 V and $(E_{1/2})^{4c}$ = −2.236 V, seen in Figure 6 as two reversible waves of low intensity yielding successively the porphyrin-based anion radical **1**$Zn^{\bullet -}$ and the dianion **1**Zn^{2-}. On the anodic side, the weakly intense and poorly reversible wave observed at ca E^{1a} = 0.682 V is attributed to the oxidation of the porphyrin ring, shifted by more than +300 mV compared to that of TPPZn (TPP : 5,10,15,20-tetrakis(phenyl)porphyrin) [48]. due to the presence of four electron-withdrawing viologen substituants. These results also stand in sharp contrast to previous studies demonstrating that the first two-electron reduction of the parent 5,10,15,20-tetrakis(*N*-methyl pyridinyl)porphyrin ($TPyPZn^{+4}$) derivatives is not centered on the peripheral pyridinium substituents but rather on the porphyrin ring to yield a porphyrin dianion ($P \rightarrow P^{2-}$) [49-54]. Such fundamental differences observed within a series of structurally related viologen-

or- pyridinium-appended porphyrin compounds can actually be attributed to the much better electron-acceptor properties of the viologen units, which therefore end-up being reduced before the porphyrin unit. Another major difference observed in the electrochemical signatures of these compounds is that the porphyrin ring gets reduced as a single two-electron wave in $TPyPZn^{+4}$ ($P \rightarrow P^{2-}$)[49, 54] and as two-successive one-electron reduction waves in $\mathbf{1}Zn^{8+}$ ($P \rightarrow P^{\bullet-} \rightarrow P^{2-}$), which suggests that the porphyrin anion radical state ($P^{\bullet-}$) is stable (at least at the CV time scale) when viologen substituents are involved.

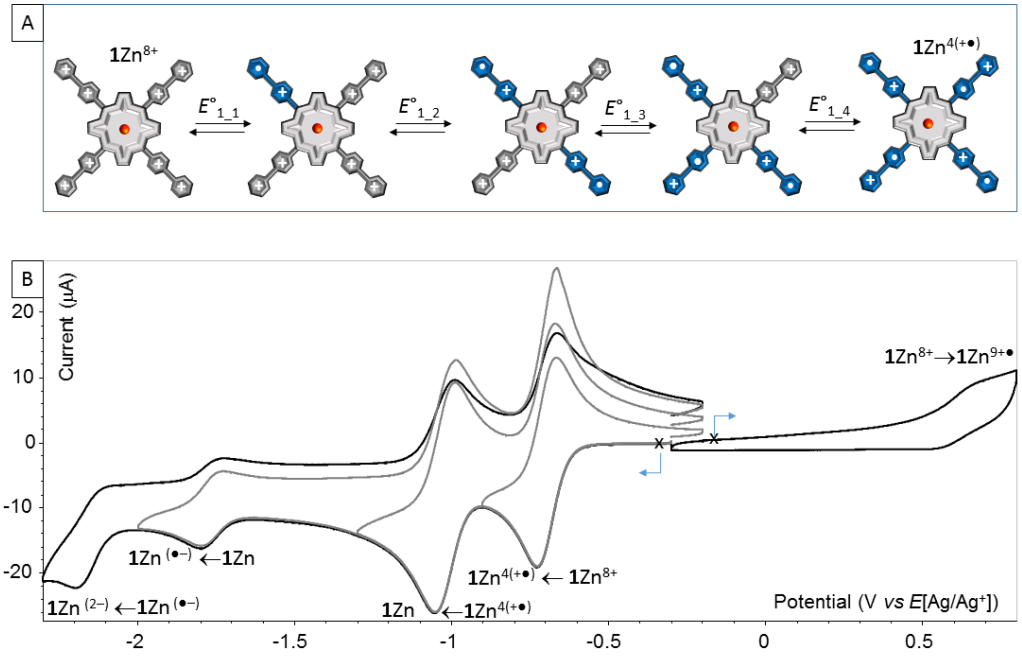

Figure 6. Voltammetric curves of a DMF (TBAP 0.1 M) solution of $\mathbf{1}Zn(PF_6)_8$ (5×10^{-4}M) recorded at a carbon working electrode (Ø = 3 mm, *E* vs Ag/Ag+ (10^{-2}M), ν = 0.1 $V \cdot s^{-1}$).

The free base porphyrin $\mathbf{1}H_2^{8+}$ was also studied in the same experimental conditions. Selected key values recorded with this compound are collected in Table 1. We found the four electron-reduced species $\mathbf{1}H_2^{(4+\bullet)}$ to be more prone to adsorption than the metalated analog but these phenomenon, revealed on the CV curves by the observation of Gaussian-shaped redissolution peaks on the backward scan, could be readily circumvented with suitable dilutions (below 2.10^{-4} M). The absence of metal in the porphyrin rings is also found to result in a significant anodic shift of the porphyrin-centered reduction waves and in the observation of a fully irreversible oxidation wave at E^{1a} = 0.728 V, which is agreement with the known electron-donating and stabilizing effect of the zinc atom on the porphyrin-based π system. The values collected in

Table 1 also reveal that the viologen-based reduction potentials are only weakly affected by the presence of the zinc ion in the cavity of the porphyrin ring.

The ability of viologen cation radicals to form non-covalent intermolecular dimers, known as π-dimers [16], in solution can be readily inferred from absorption spectroscopy measurements, most notably through the observation of a diagnostic broad absorption bands in the near infra-red region whose energy is proportional to the electronic coupling term arising from frontier-orbital interactions between a pair of equivalent SOMOs [23]. The signature of the reduced forms of **1**Zn^{8+}, and their ability to self-assemble in DMF solutions, has thus been carefully investigated by spectroelectrochemistry, which involved regularly recording absorption spectra over time during bulk reductions carried out in potentiostatic regimes. The exhaustive electrolysis (1e/viologen) of **1**Zn^{8+} ($5.7x10^{-5}$ M) carried out at in DMF at a platinum electrode led to a slight broadening of the porphyrin-based Soret band coming along with a significant bathochromic shift, of about 7 nm, of its maximum wavelength (from 426 to 433 nm with a clean isosbestic point at 429 nm, see **Figure 7**A). The extent of these modifications is fully compatible with electron transfers centered on the peripheral viologens having a minor impact on the electron density of the porphyrin-based π-system. This attribution is further supported by the emergence of intense absorption bands between 500 and 800 nm, overlying with the porphyrin-based Q bands, attributed to a series of transitions centered on a viologen cation-radical, as revealed by the good match with the spectrum of the radical electrogenerated from the reference *N*,*N*-dimethyl viologen (Me**V**$Me^{+\bullet}$, see dash-dotted line in **Figure 7**). The main findings of this preliminary study are thus that the conversion **1**Zn^{8+} →**1**$Zn^{(4+\bullet)}$ is fully reversible at the electrolysis time scale (30 min) and that the electrogenerated species **1**$Zn^{(4+\bullet)}$ do not form π-dimers in these experimental conditions, as revealed by the absence of diagnostic absorption bands in the near IR region (~900 nm) and by the standard ΔE_p value of about 60 mV measured on the first viologen-based CV wave.

Further investigations carried out on the free base **1**H_2^{8+} led to similar findings with a spectroscopic signature recorded after bulk electrolysis at E_{ap} = -0.85 V (*vs* $E_{ref}[Ag/Ag^+]$) in agreement with the formation of the tetra-radical species **1**$H_2^{(4+\bullet)}$ (**Figure 7**B).

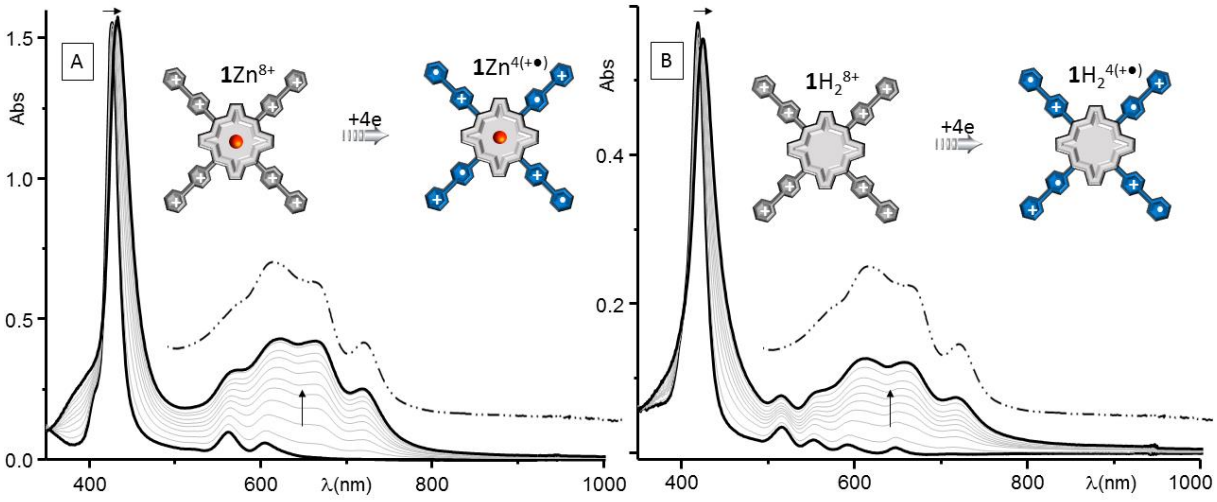

Figure 7. UV−vis spectra recorded during the exhaustive one-electron reduction (per viologen) of A) **1**Zn$(PF_6)_8$ (5.7 10^{-5} M) and B) **1**$H_2(PF_6)_8$ (2 10^{-5} M) in DMF (0.1 m TBAP) using a platinum plate working electrode whose potential was fixed at E_{ap} = −0.85 V vs $E_{Ag/Ag+}$ (10 mL, l = 1 mm, t = ∼30 min).

Table 1. Potential values measured by cyclic voltammetry for Me**V**Me^{2+}, **1**Zn^{2+} and **1**H_2^{2+} in aqueous and organic media. The number of electrons transferred and the peak to peak potential shift ($\Delta E_P = E_{pa}$-E_{pc} (mV)) for each electrochemical process is shown between parentheses. X = PF_6^-, Y = Cl^-.

		E^{4c}(n, ΔE_P) **$P^{\bullet-}/P^{2-}$**	E^{3c}(n, ΔE_P) **$P/P^{\bullet-}$**	E^{2c}(n, ΔE_P) **$V^{+\bullet}/V^0$**	E^{1c}(n, ΔE_P) **$V^{2+}/V^{+\bullet}$**	E^{1a}(n, ΔE_P) **($P^+/P^{+\bullet}$)**
Me**V**Me$(X)_2$	DMF	na	na	-1.163[b] (1,62)	-0.774[b] (1,60)	na
1$H_2(X)_8$	DMF	-2.011[b] (1,84)	-1.613[b] (1,84)	−1.115[b] (4,77)	−0.785[b] (4,60)	0.728[c] (1)
1Zn$(X)_8$	DMF	-2.236[b] (1)	−1.827[b] (1,75)	−1.087[b] (4,67)	−0.762[b] (4,63)	0.682[c] (1)
Me**V**Me$(Y)_2$	H_2O	na	na	-0.996 (1,77)[b]	−0,654(1,60)	na
1Zn$(Y)_2$	H_2O	na	no	-0.638 (4,24)	−0,389[c,d]	0,861[c] (1)

Measured by CV, 2-5·10^{-4} M in DMF/TBAP (0.1 M, E(V) vs. Fc/Fc^+), or in an aqueous phosphate buffer (0.1M, pH = 7, E(V) vs. Ag/AgCl (KCl sat)) at a vitreous carbon working electrode Ø = 3 mm, 298 K, ν = 0.1 V·s^{-1}.
na : Not available
[b] : Half wave potential
[c] : Peak potential
[d] : Adsorption phenomena

Table 1. Potential values measured by cyclic voltammetry for Me**V**Me^{2+}, **1**Zn^{2+} and **1**H_2^{2+} in aqueous and organic media. The number of electrons transferred and the peak to peak potential shift ($\Delta E_P = E_{pa}$-E_{pc} (mV)) for each electrochemical process is shown between parentheses. X = PF_6^-, Y = Cl^-.

Electrochemistry in aqueous medium

All the studies described below have been conducted on the metalated compound **1**Zn^{8+} only, as its signature and stability in aqueous medium proved best suited for reaching the targeted objectives. The idea here was to investigate the ability of CB[8] to promote the intermolecular dimerization of the four-electron reduced species **1**$Zn^{(4+\bullet)}$ in water to yield 2D self-assemblies (Figure 8), as opposed to CB[7] expected to form only discrete host-guest caviplexes with **1**$Zn^{(4+\bullet)}$.

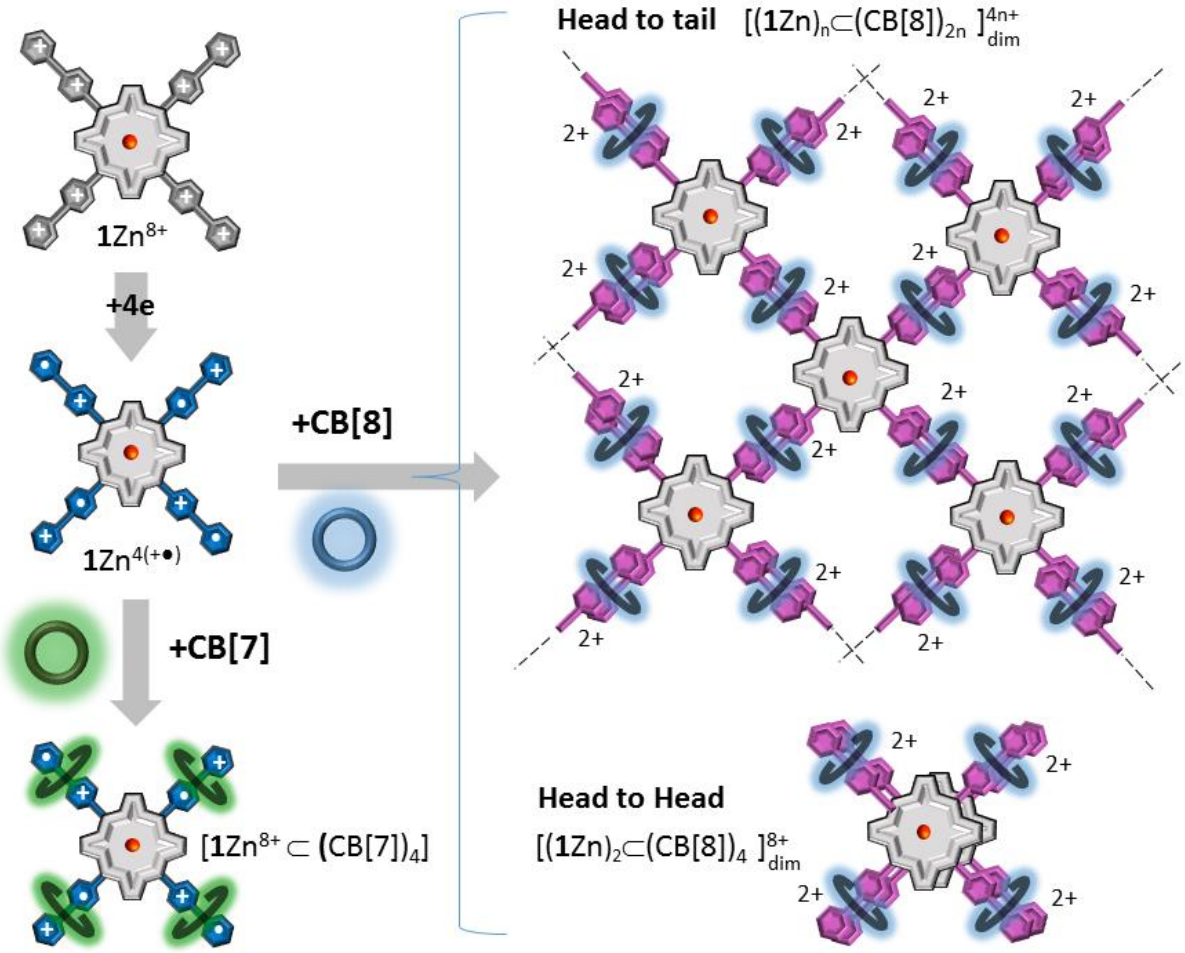

Figure 8. Schematic drawing showing the expected binding modes between the four-electron reduced species **1**$Zn^{(4+\bullet)}$ and CB[n], with n = 7 or 8.

The electrochemical behavior of the reference compound Me**V**Me^{2+} in the presence of cucurbit[n]urils has been described by several authors [55-58]. These seminal contributions have served to establish that viologen-based π-dimers can be stabilized in the cavity of CB[8] but not in that of the smaller analog CB[7], only capable of forming 1/1 inclusion complexes with viologen derivatives (as dications or radical cations). From an electrochemical point of

view, the formation of Me**V**Me^{2+} ⊂ CB[n] in aqueous electrolytes is usually revealed by significant shifts of the viologen-based reduction waves coming along with marked decreases in the current levels. As a general statement, the extent of the potential shifts induced upon binding can be related to the relative affinity of the barrel-shaped host for the dicationic, radical-cationic or neutral/quinonic species produced at the electrode interface. The much larger affinity of CB[7] for Me**V**Me$^{+\bullet}$ than for Me**V**Me^{0} is for instance revealed by a significant shift of the second reduction wave (Me**V**Me$^{+\bullet}$/ Me**V**Me^{0}, ΔE<-100 mV), while its similar affinity for Me**V**Me$^{+\bullet}$ and Me**V**Me^{2+} accounts for a limited displacement of the first reduction waves (Me**V**Me^{2+}/ Me**V**Me$^{+\bullet}$, ΔE ~-25 mV) [58]. Further studies have shown that the stabilization of the Me**V**Me$^{+\bullet}$ redox state through π-dimerization ($2Me\mathbf{V}Me^{+\bullet} \rightarrow [(Me\mathbf{V}Me^{+\bullet})_2]_{dim}$) inside the cavity of CB[8] results in a cathodic shift of the first reduction wave (Me**V**Me^{2+}/Me**V**Me$^{+\bullet}$, ΔE ~-150 mV) associated to a concomitant cathodic shift of the second reduction wave (Me**V**Me$^{+\bullet}$/Me**V**Me^{0}, ΔE <-250 mV) [56]. To summarize, all these studies have brought to light that key information on the inclusion of viologens, in all their redox states, within CB[n] can be obtained from electrochemical measurements.

The electrochemistry of the title tetraviologen guest **1**Zn^{8+} has thus been investigated in a phosphate buffer (pH 7, 0.1 M) at a vitreous carbon electrode. The most relevant data recorded for this compound in the absence of CB[n] are collected in Table 1. On the anodic side, the oxidation of the porphyrin is observed as an irreversible CV wave at E^{1a} = 0.861 V. In contrast to what is seen in organic media, both consecutive viologen-based reduction waves observed in water at E^{1c} = −0,389 and E^{2c} = −0,638 V are found to be associated on the reverse scan to Guaussian-shaped reoxidation peaks attributed to the anodic redissolution of physisorbed species (see Figure ESI 11). As expected, such phenomenon was found to be particularly important for the neutral and hydrophobic porphyrin-based complex **1**Zn^{0}, involving quinonic V^{0} substituants, electrogenerated at E^{2c} = −0,638 V. A systematic study carried out with different electrolytes allowed us to establish that the adsorption of the first tetracationic compound **1**Zn$^{4(+\bullet)}$ can be significantly reduced upon lowering the concentration of **1**Zn^{8+} down to 2.10^{-4} M and upon increasing the scan rate of the CV measurement, as revealed by the linear $I_{peak} = f(\nu^{1/2})$ plot recorded on the first reduction wave for $\nu \geq 400$ mV/s (see Figure ESI 10).

The interaction with CB[8] have been investigated in these experimental conditions upon recording the changes in the viologen-based signature induced by formation of the inclusion compounds [**1**Zn^{8+} ⊂ **(**CB[8])$_n$]. The curves shown in **Figure 9**, focusing on the first viologen-based reduction wave, have been recorded at different CB[8]: **1**Zn^{8+} ratio (from 0 up to 2). It

needs to be mentioned here that the upper value of the molar ratio reached towards the end of the titration, CB[8]: **1**Zn^{8+} = 2, not only corresponds to the ratio needed to form the ideal 2D arrangement shown in Figure 8, it was also found to be the solubility limit of CB[8] in our experimental conditions. The CV curves depicted in **Figure 9**A, recorded after addition of 0/0.25/0.5/0.75 molar equivalents of CB[8], reveal that the in-situ formation of partially complexed compounds [**1**Zn^{8+} ⊂ **(**$CB[8])_n$] (with $n \leq 0.75$) results in the progressive disappearance of the initial reduction wave at –0.389 V at the expense of a new reduction wave emerging at a less negative potential. This trend prevails up to the end of the titration, when reaching the maximum concentration of CB[8] (2 molar equivalents, see **Figure 9**B), with the observation of a new wave attributed to the reduction of the inclusion complex [**1**Zn^{8+} ⊂ **(**$CB[8])_2$] at E_p = –0354 V. These changes are moreover seen to come along with a significant loss in the peak-current values measured on the forward and backward scans, which is in agreement with the formation of much larger species featuring lower diffusion coefficients. The formation of host-guest complexes involving both the V^{2+} and $V^{+\bullet}$ redox states of the appended viologen is further revealed by the ability of CB[8] to prevent the physisorption of the four-electron reduced species, as demonstrated by the progressive loss of the Gaussian character associated to the reoxydation peak observed prior addition of CB[8]. Such evolution is indeed consistent with the formation of inclusion species with limited affinity for the electrode surface at the CV time scale, as demonstrated by the linearity of the $I_{peak} = f(\nu^{1/2})$ curve recorded after addition of 2 molar equivalents of CB[8] (see Figure ESI 10). The stabilization of the viologen cation radical as dimers included in CB[8] is further revealed by the large shift, reaching -400 mV by the end of the titration, of the second viologen-centered reduction leading the neutral quinonic form of the viologens ($V^{+\bullet} \rightarrow V^0$, see Figure ESI 11). As mentioned in the introduction about literature data [56], such effect of CB[8] is consistent with an extension of the stability domain of the cation radicals state on account of π-dimerization, which end up being easier to produce (anodic shift of the first reduction potential) and harder to consume (cathodic shift of the second reduction potential).

Overall, the formation of inclusion complexes with CB[8] has been found to have a major impact on the potential values and on the current levels. As just mentioned above about the behavior of the reference compound Me**V**Me^{2+}, the changes observed in **Figure 9**A/B are consistent with a CB[8]-assisted intermolecular π-dimerization of the viologen-based cation radicals. On purely sterical grounds, it can be stated that such process can only lead to the formation of self-assembled supramolecular structures involving head to tail viologen-based π-

dimers (see Figure 8, one methyl and one phenyl substituent on each side of the CB cavity). This key assumption, implying that the formation of the most symmetrical head to head conformation (Figure 8) is prevented by sterical clashes, has been checked by DFT calculation carried out on a model compound (see **Figure 15**B and the associated discussion in the computational section).

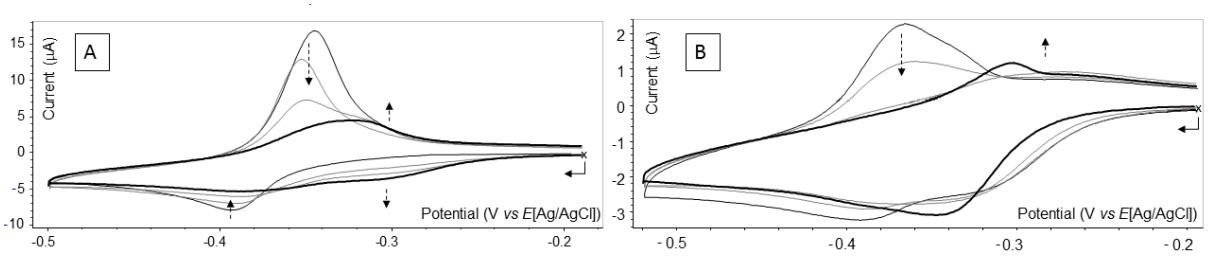

Figure 9. Voltammetric curves of an aqueous (phosphate buffer, 0.1 M) solution of **1**Zn$(PF_6)_8$ (2×10^{-4}M) recorded at a non-stationary carbon working electrode (Ø = 3 mm, *E*(V) vs. Ag/AgCl, 50 mV/s (A) or 100 mV/s (B)) after addition of increasing amounts of CB[8] : A) 0/0.25/0.5/0.75 molar equivalents and B) 1/1.25/1.5/2 molar equivalents.

The formation of self-assembled supramolecular architectures $[(\mathbf{1}Zn)_n \subset (CB[8])_{2n}]^{4n+}$ through iterative CB[8]-assisted π-dimerization of the viologen cation radicals in $\mathbf{1}Zn^{4(+\bullet)}$ has been further demonstrated upon carrying out the same investigations with CB[7], whose cavity dimension precludes the formation of such dimers.

The CV curves recorded after addition of increasing amounts of CB[7] are collected in **Figure 10** and in Figure ESI 12. As opposed to what was found with CB[8], the formation of $[(\mathbf{1}Zn) \subset (CB[7])_n]^{8+}$ ($1 \leq n \leq 4$) results in the progressive shift of the reduction potential towards more negative potential values along with a drop of the current levels. Such behavior is here again fully consistent with previous studies carried out with Me**V**Me^{2+} showing that such such cathodic shift can be attributed to the similar affinity of CB[7] for the dication Me**V**Me^{2+} (K_1= 2 10^5) and for the electrogenerated cation radical Me**V**Me$^{+\bullet}$ (K_1= 8.5 10^4) [58]. A similar conclusion can thus be put forward to account for the modification of the CV data recorded in the presence of $\mathbf{1}Zn^{8+}$ and CB[7].

As a conclusion, the electrochemical data discussed above support the conclusion that the anodic shift of the first reduction wave observed in the presence of CB[8] is attributed to the stabilization of the electrogenerated viologen cation radicals as intermolecular π-dimers, while CB[7] forms stable 1/1 complexes with both the dicationic and cation-radicals states of the viologen guests**.**

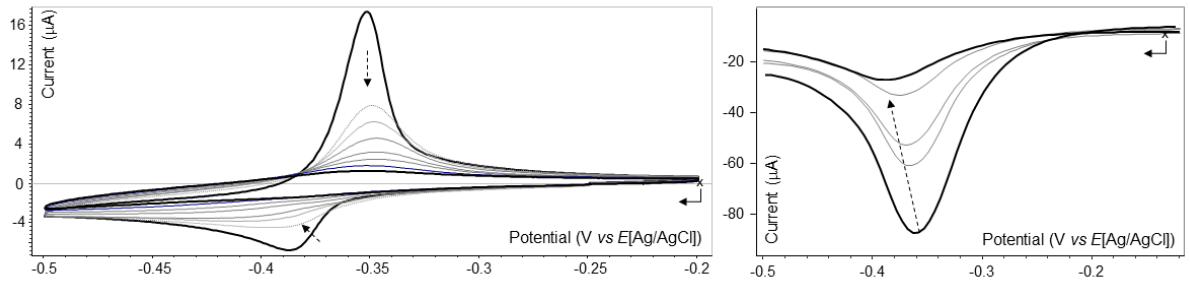

Figure 10. Voltammetric curves of an aqueous (phosphate buffer, 0.1 M) solution of $1Zn(PF_6)_8$ (2×10^{-4}M) recorded at a non-stationary carbon working electrode (Ø = 3 mm, *E*(V) vs. Ag/AgCl, 50mV/s) after addition of increasing amounts of CB[7] A) 0/1/1.5/2/2.5/3/3.5/4 molar equivalent.

The CB[8]-promoted π-dimerization of the 4-electron-reduced species $\mathbf{1}Zn^{4(+\bullet)}$ yielding self-assembled supramolecular systems conforming to the general formula $[(\mathbf{1}Zn)_n \subset (CB[8])_{2n}]_{dim}^{4n+}$ has been confirmed with spectroscopic measurements carried out in water in the presence of chemical reductants. Preliminary attempts to generate the reduced species by bulk electrolysis at reticulated vitreous carbon foam electrodes failed due to the significant adsorption of the reduction products, even though no such process was observed at much shorter time scales over the course of CV analyses.

The one-electron reduction of the viologen units in $\mathbf{1}Zn^{8+}$ was thus carried out in phosphate buffer (pH =7) using sodium dithionite $Na_2S_2O_4$ as a reductant [59]. The UV-Vis absorption spectra recorded over time in the presence of CB[8] after addition of $Na_2S_2O_4$ in excess are shown in **Figure 11**A. These curves reveal that the chemical reduction has very little impact on the soret band centered at 421 nm, as expected for electron transfers centered on the peripheral viologens ($V^{2+} \rightarrow V^{+\bullet}$) and not on the porphyrin ring. It conversely leads to the development of two intense absorption bands at λ_{max} = 560 and 634 nm coming along with a less intense signals centered at 918 nm. The attribution of those signals could be achieved through comparison with the spectra of structurally related reference compounds, namely the viologen-based radical $\mathbf{5}^{+\bullet}$ and the pure π-dimer $[(\mathbf{6})_2]_{dim}^{2+}$ (blue and purple drawings and curves in **Figure 11**) [18]. One key conclusion drawn from this analysis, and more particularly from the perfect matching between the spectrum of $[(\mathbf{6})_2]_{dim}^{2+}$ and that recorded after reduction of $\mathbf{1}Zn^{8+} \subset (CB[8])_2$ with $Na_2S_2O_4$, is that the viologen radicals in the chemically reduced species $\mathbf{1}Zn^{4(+\bullet)}$ are involved in the formation of intermolecular π-dimers. Both spectra indeed feature an intense charge-resonance absorption band observed in the NIR region, at λ_{max} = 918 nn, which is a typical feature of viologen-based π-dimers attributed to the electronic transition from the bonding to the antibonding π orbitals resulting from the interaction between two identical cation radicals.

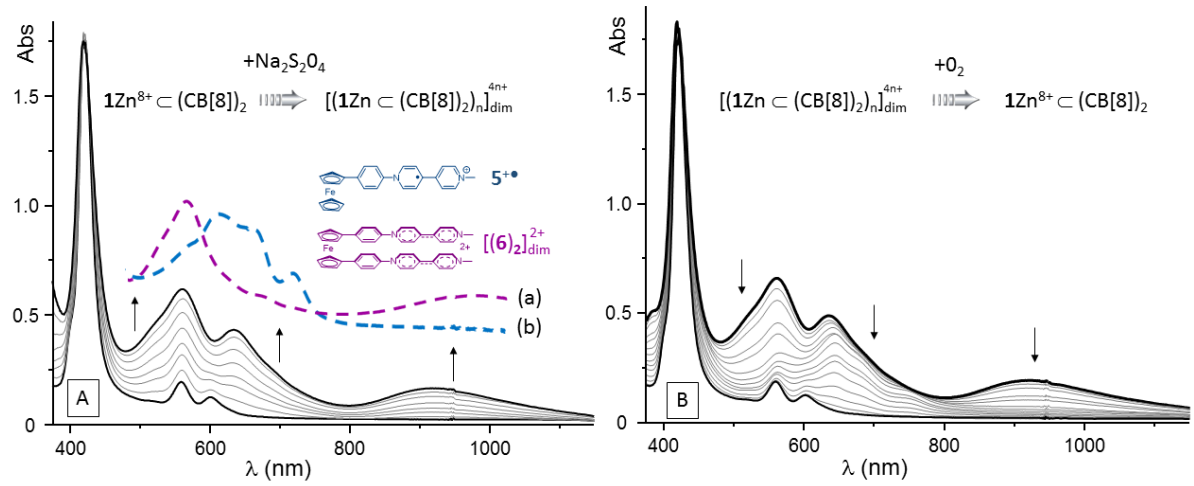

Figure 11. UV−vis spectra of **1**Zn(PF$_6$)$_8$ (1.110^{-5} M) and CB[8] (2 molar equivalents) in phosphate buffer (pH 7, 0.1 M) recorded over time after addition of $Na_2S_2O_4$ in excess (A) and followed by gentle bubbling of compressed air (B).

In solution, such long-bonded dimer are most of the time found in equilibrium with the non-associated cation radicals. In our case, the presence of free cation radicals in solution is revealed by the third signal growing at λ_{max} = 634 nm, which is similar to the signature of the "free radical" reference compound **5**$^{+\bullet}$ (**Figure 11**A). The spectroscopic data collected over the four-electron reduction of **1**Zn^{8+}⊂ (CB[8])$_2$ with $Na_2S_2O_4$ are thus consistent with the formation of self-assembled supramolecular structure $[(\mathbf{1}Zn)_n{\subset}(CB[8])_{2n}]_{dim}^{4n+}$ built from a CB[8]-promoted intermolecular dimerization of the viologen cation radicals present in **1**Zn$^{4(+\bullet)}$. Another key feature of the proposed supramolecular assembly is its fully dynamic and reversible nature. The ability to dissociate the self-assembled system $[(\mathbf{1}Zn)_n \subset (CB[8])_{2n}]_{dim}^{4n+}$ and to regenerate the initial inclusion complex **1**Zn^{8+} ⊂ (CB[8])$_2$ was readily checked upon bubbling compressed air through the solution. The slow re-oxidation of the viologen-based radicals, and the concomitant dissociation of the CB[8]-stabilized supramolecular dimers, are both revealed in **Figure 11**B by the progressive disappearance of the intense bands attributed to $[(\mathbf{1}Zn)_n \subset (CB[8])_{2n}]_{dim}^{4n+}$ at the expense of the initial Q-bands of **1**Zn^{8+}⊂ (CB[8])$_2$ whose intensities are fully recovered by the end of the experiment. The redox-triggered self-assembly process thus proved fully reversible but a close examination of the spectra depicted in **Figure 11**A and **Figure 11**B clearly suggest that the coupled electrochemical-chemical (E_nC_n) pathways taken over the course of the reduction and re-oxydation processes are different. The first stage of the reduction process (**Figure 11**A) indeed sees the accumulation of π-dimerized species (λ_{max} = 560 and 918 nm) followed by that of free un-associated radicals (λ_{max} = 634 nm) while the reoxydation (**Figure 11**B) leads first to the consumption of the dimers followed by that of the non-associated radicals. In support of these conclusion, we found that a well-defined, dimer free, signature of

free radical species can only be observed by the end of the re-oxidation process, after consumption (reoxidation) of all the π-dimerized compounds. The discrepancies observed between the reduction and oxidation pathways are not yet fully understood but the sequence of events in both cases is clearly imposed by the CB[8]-promoted stabilization of the viologen cation radical as dimeric compounds.

Similar experiments have then be carried out in the absence of CBs (Figure 12) and in the presence of CB[7] (Figure 13) to provide further support for the proposal that the CB[8] hosts promote the formation of supramolecular dimers. The chemical reduction of **1**Zn^{8+} alone and its subsequent re-oxydation with O_2 are shown in Figure 12A and Figure 12B, respectively. What strikes at first sight is *i*) the total reversibility of the reduction/oxidation cycle and *ii*) the major differences between these data and those recorded in the same conditions with CB[8]. Reduction of the "free" guest molecule **1**Zn^{8+} has for instance a major impact on the Soret band, experiencing in Figure 12A a loss of about 1/3 of its initial intensity together with a blue shift of about 13 nm of the maximum wavelength, going from 420 to 407 nm with a well-defined isobestic point at 413 nm. These differences also include the emergence of a series of new bands centered at 518 (sh), 550 and 622 nm coming along with a very broad and weakly intense signal at λ_{max} = 1050 nm. Another key output is that the exact same spectroscopic signatures has been observed in the same conditions with **1**Zn^{8+} alone and with the CB[7] threaded caviplex **1**Zn^{8+} ⊂ $(CB[7])_4$ (see Figure 12A and Figure 13A).

Taken together all these data support the conclusion that the chemical reduction of **1**Zn^{8+} or **1**Zn^{8+}⊂ $(CB[7])_4$ with an excess of $Na_2S_2O_4$ results in the concomitant reduction of the viologen substituants ($V \rightarrow V^{+\bullet}$) and of the porphyrin ring ($P \rightarrow P^{\bullet-}$). There is limited literature on porphyrin anion radicals and porphyrin dianions but some studies conducted in aqueous on the parent 5,10,15,20-tetrakis(N-methyl pyridinyl)porphyrin ($TPyPZn^{+4}$) proved useful to put forward a global interpretation of the observed phenomena. The latter have for instance established that the π-anion radical ($P^{\bullet-}$) of $TPyPZn^{+4}$ (λ_{max} ~700-750 nm)[60-62] is unstable in solution and quickly evolves, through a bimolecular disproportionation process occuring at the millisecond time scale, into a porhyrin dianion (P^{2-}) which is in turn readily transformed at neutral pH into a protonated species termed phlorin (PH^-) featuring one sp^3-hybridized *meso* carbon atom [60, 63-67]. It should also be mentioned that the driving force of this overall EC_2 process ($P \rightarrow P^{\bullet-} \rightarrow P^{2-} \rightarrow PH^-$) is so strong that it can also be observed in aprotic polar organic solvent polluted with water molecules. Another specific feature relevant to the experimental data shown in Figure 12 and Figure 13 is that the formation of phlorin anions from porphyrins

is a reversible process, the latter being usually fully regenerated ($PH^{-} \rightarrow P$) by simple electrochemical or chemical re-oxidation of the sample [63, 68, 69, 70 , 71]. In terms of characterization, phlorins are known to more easily reduced than porphyrins ($E°[PH/PH^{-}] > E°[P/P^{\bullet -}]$). Their formation is most of the time revealed by absorption spectroscopy through the observation of a broad absorption band developing in the near IR region (>700 nm, with feature depending on the central metal and on the *meso*-substituents) and by the disappearance of the initial Soret band at the expense of a much weaker and broader signal developing at longer wavelengths ($\Delta\lambda$~+30 nm and $\varepsilon_P/\varepsilon_{PH}$ ~7 for ZnTPP) [71].

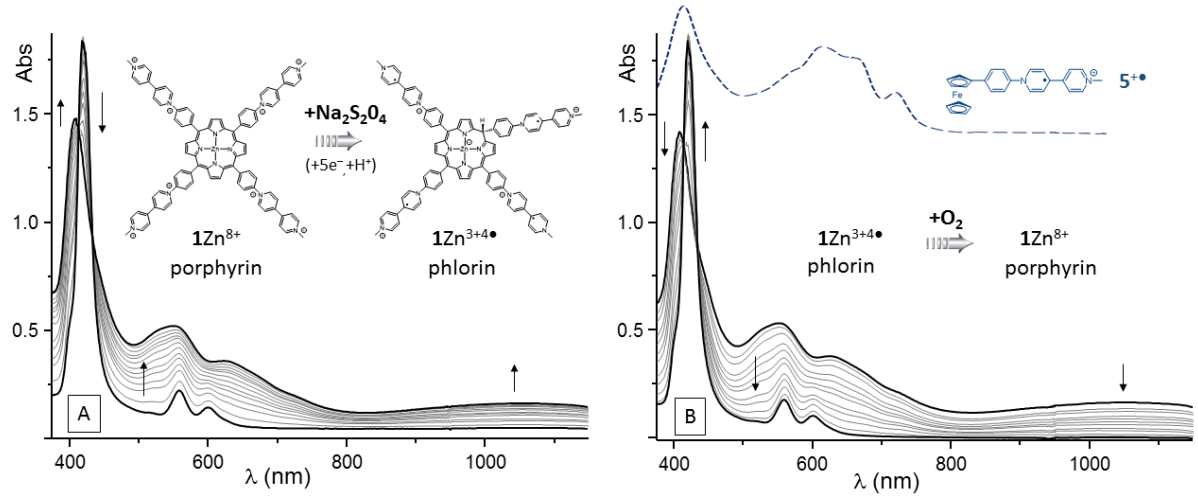

Figure 12. UV−vis spectra of $1Zn(PF_6)_8$ ($1.1\ 10^{-5}$ M) in phosphate buffer (pH 7, 0.1 M) recorded over time after addition of $Na_2S_2O_4$ in excess (A) and followed by gentle bubbling of compressed air (B).

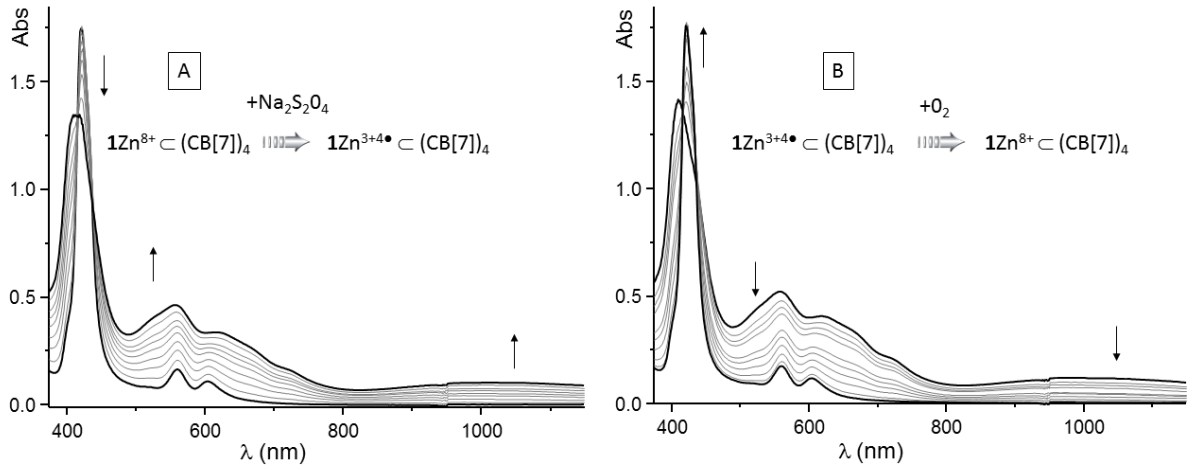

Figure 13. UV−vis spectra of $1Zn(PF_6)_8$ ($1.1\ 10^{-5}$ M) and CB[7] (4 molar equivalents) in phosphate buffer (pH 7, 0.1 M) recorded over time after addition of $Na_2S_2O_4$ in excess (A) and followed by gentle bubbling of compressed air (B).

All this literature demonstrating the instability of porphyrin anions radicals in protic media support our conclusion that the unexpected behavior recorded with $\mathbf{1}Zn^{8+}$ and $\mathbf{1}Zn^{8+} \subset (CB[7])_4$ is attributed to the formation of a phlorin product (noted $\mathbf{1H}Zn^{3+4\bullet}$ in Figure 12), incorporating

four viologen cation radicals and a negatively charged *meso*-protonated phlorin ring (Figure 12A). Such finding implies that, in our experimental conditions, $Na_2S_2O_4$ is capable of reducing the viologen cation radical and the porphyrin ring. The involvement of the porphyrin ring in the electron transfer is here unambiguously demonstrated by the disappearance of the initial Soret band at the expense of a less intense and blue shifted signal centered at 407 nm, whose features are reminiscent of that observed in the same range on the spectrum of the reference viologen cation radical $5^{+\bullet}$ (shown as a blue curve in Figure 12B). The presence of viologen cation radicals is thus clearly revealed in Figure 12A and Figure 13A by the emergence of a signal centered at 407 nm together with multiple signals above 600 nm. Formation of a phlorin-type of product is conversely demonstrated by i) the disappearance of the initial Soret band, ii) by the development of a broad band in the NIR region iii) by the observation of a shoulder at ~450 nm and by iii) the full regeneration of the initial porphyrin by simple re-oxygenation of the reduced sample.

This interpretation was further confirmed with additional experiments showing that similar signatures can be obtained when using tetrakis(dimethylamino)ethylene [72] as a reducing agent or using light in the presence of a suitable electron donor [11, 73]. The latter procedure involved irradiation at λ_{ex} = 455 nm of the investigated solutions containing tris(bipyridine) ruthenium chloride as a photosentisizer (0,1 mM) and ethylenediaminetetraacetic acid (EDTA, 0,1 M) as a sacrificial electron donor [74]. The absorption spectra recorded during irradiation are shown in **Figure 14**. Here again the signal centered at ~ 900 nm, attributed to the formation of intermolecular viologen-based π-dimers, is observed only in the presence of CB[8] (**Figure 14**A), the photoreduction of **1**Zn^{8+} and **1**$Zn^{8+} \subset (CB[7])_4$ leading to the observation of different signals attributed to the reduction of the porphyrin ring (**Figure 14**B). It should be noted that all our attempts to reduce the viologen units using the porphyrin ring as the photosensitizer (λ_{ex} = 365 or 455 nm) failed, most probably due to the efficient and fast recombination of the charge separated intermediates.

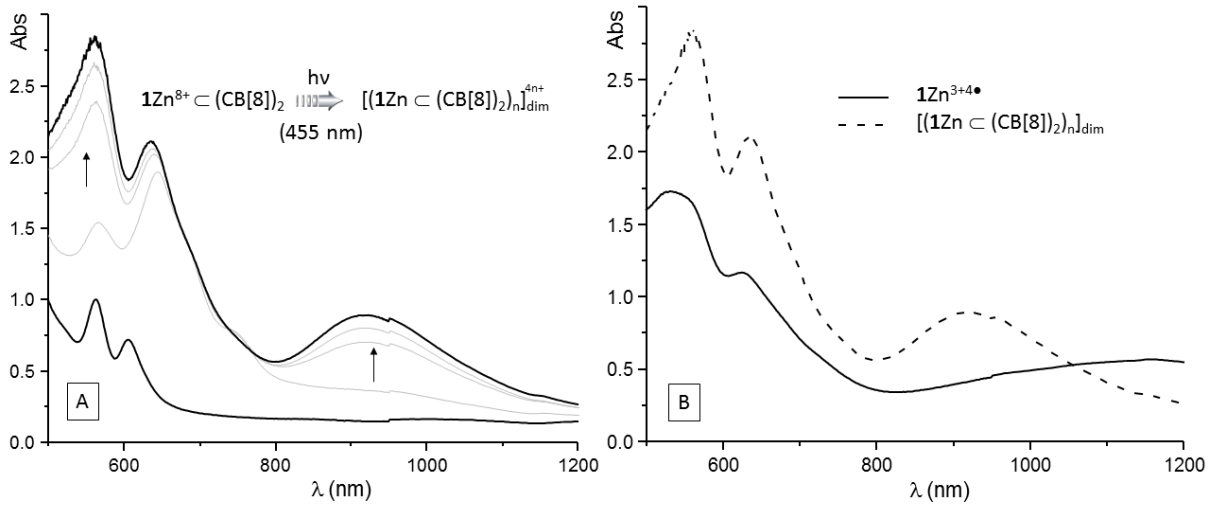

Figure 14. (A) UV−vis spectra of $1Zn(Cl^-)_8$ ($1\ 10^{-4}$ M) and CB[8] ($2\ 10^{-4}$ M) in phosphate buffer (pH 7, 0.1 M) recorded during irradiation at λ_{ex} = 455 nm (B) Comparison of UV−vis spectra of $1Zn(Cl^-)_8$ ($1\ 10^{-4}$ M) in absence (plain line) and presence of CB[8] ($2\ 10^{-4}$ M) (dotted line) in phosphate buffer (pH 7, 0.1 M) recorded during irradiation at λ_{ex} = 455 nm.

Overall, the photo or chemical reduction experiments discussed above lead to the same experimental data consistent with the conclusion that CB[8] *i*) promotes the intermolecular dimerization of the viologen cation radicals and *ii*) prevents the reduction of the porphyrin ring.

Computational analysis

The ability of CB[8] to assist the π-dimerization of **1**Zn^{8+} has been investigated by quantum chemistry calculations carried out on a simple model featuring only one viologen guest linked to a zinc-bearing porphyrin ring (**Figure 15**). A geometry optimization has been conducted on the self-assembled π-dimers formed at the reduced state (one electron per viologen) in the presence of CB[8] to evaluate the structural and energetical impacts of the CB[8] cavitand on the dimer, to gain insights into its stabilization energy and into the relative position of the porphyrin and viologen subunits. Geometries have been optimized at the GGA hybrid Truhlar's density functional DFT/M06-2X level of theory [75], with a basis set 6-31G(d,p) using the Gaussian 16 revision B.01 suite of programs. This density functional is best suited to account for the dispersion interactions involved in π-dimers [26, 76] and comes with a high percentage of exact exchange which is a needed feature to describe π-radicals [13].

Preliminary calculations carried out on the two possible head to tail and head to head conformers shown in **Figure 15** led to the conclusion that the head to head conformation is disfavored by steric clashes arising between the phenyl linkers. A detailed optimization has thus been carried out starting from an ideal "head to tail" π-dimer model (two viologen cation radicals perfectly aligned sitting on top of each other at a contact distance of 3.4 Å) stabilized within the cavity of a CB[8] host. The structure obtained after optimization is shown in **Figure**

15(a, b). The phenyl ring ends up being tilted with respect to the porphyrin and viologen-based mean planes (44°) as a result of the steric repulsion occurring between the hydrogen atoms of the phenyl ring (H_f, H_g in in **Figure 15**) and those located on the porphyrin (H_h) and viologen units (H_e).

This optimized structure also reveals that both viologen radicals adopt a slightly staggered conformation with an twist angle of about 36° imposed by the steric hindrance between the N-Methyl substituent and the phenyl linker. It should however be mentioned that the energy difference calculated between this partially "staggered" optimized conformation and the perfectly aligned structure does not exceed 3.0 kcal.mol^{-1}. Such small difference suggests that the inclusion complex oscillates at room temperature between the two absolute minima centered at -36° and +36°. Similar calculations carried out on the twisted (36°) vs. parallel conformers of a less bulky dimer, involving two *N*,*N*′-dimethyl-4,4′-bipyridinium radical cation (Me**V**Me$^{+\bullet}$) bound within a CB[8] host, led to a higher energetic difference reaching 6.4 kcal.mol^{-1} (-10.0 kcal.mol^{-1} vs. -16.4 kcal.mol^{-1}) [5].

Further DFT level calculations have been carried out on the inclusion complex [**1**Zn^{8+} ⊂ **(**CB[8])$_4$] to gain insights into the spatial constraints arising between the CB[8] units surrounding the porphyrin core and also between the CB[8] rings and the porphyrin skeleton. The minimized structure shown in **Figure 16** bring to light the absence of steric hindrance between all these bulky units, as revealed by the fact that the shortest hydrogen…hydrogen interatomic distance measured on this structure is 3.32 Å, which is large enough to avoid the existence of repulsive interaction.

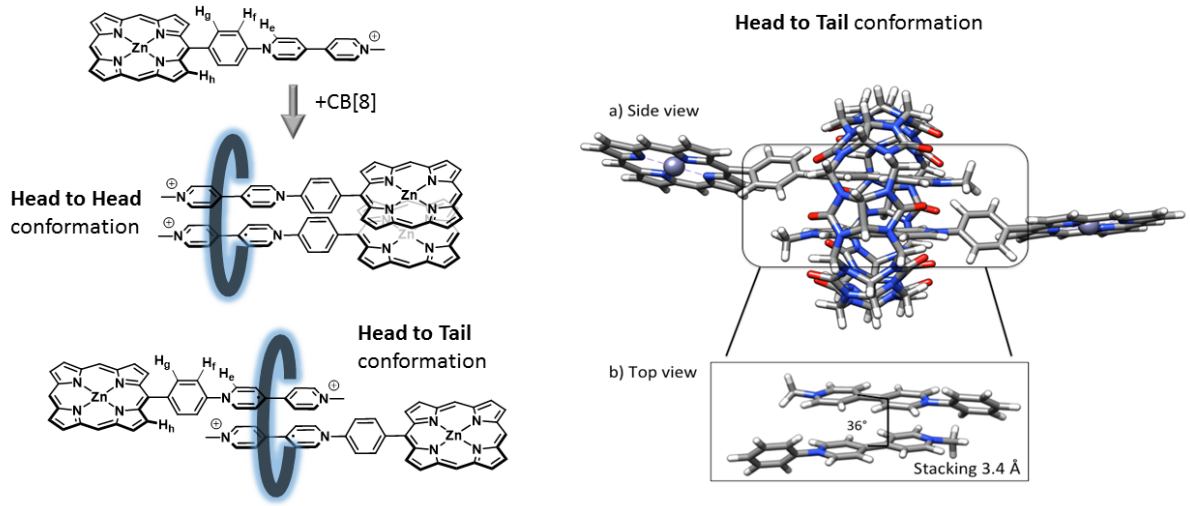

Figure 15. Left) Schematic representation of the face to face or head to tail conformations of the selected π-dimer model complex formed in the presence of cucurbit[8]uril (shown as a blue ring). Right) Structure of the head to tail conformer optimized at DFT/M06-2X level of theory

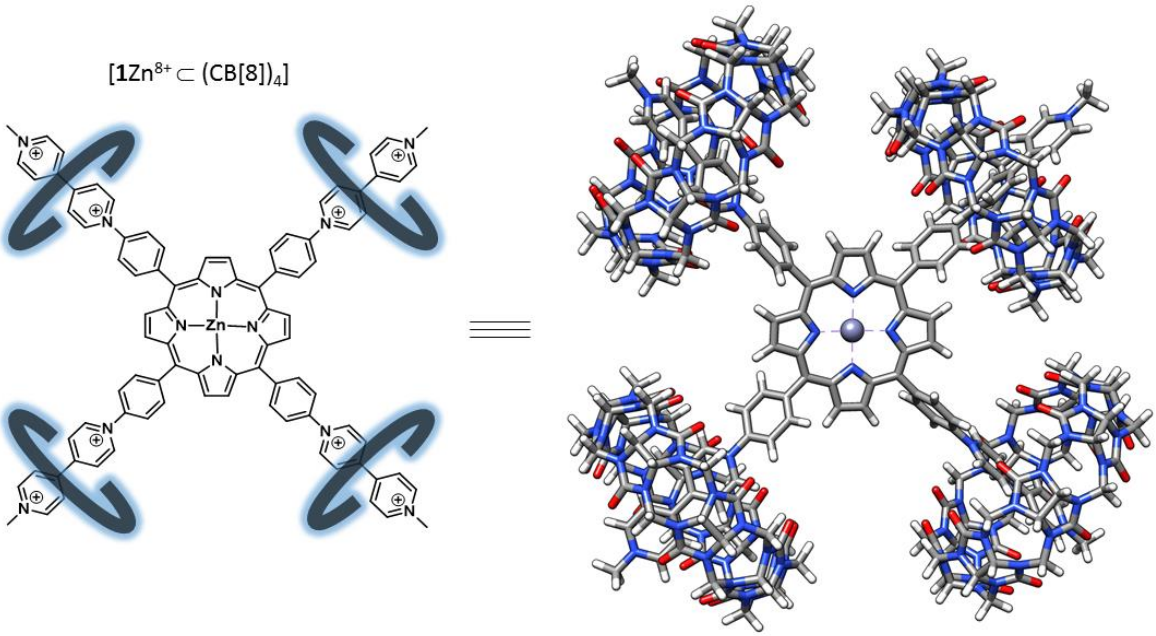

Figure 16. Left) Schematic representation of the inclusion complex [1Zn □□(CB[8])4]8+ formed in solution upon mixing 1Zn8+ with an excess of CB[8]; Right) Structure of the complex optimized at the GGA hybrid Truhlar's density functional DFT/M06-2X level of theory, with a basis set 6-31G(d,p) using the Gaussian 16 revision B.01 suite of programs.

Conclusion

Formation of discrete 4:1 pseudo-rotaxane-like caviplexes, involving threading of 4 CB[n] rings on a viologen-based four-pointed star-shaped guest molecule, has been demonstrated by NMR and MS measurements. Detailed electrochemical, theoretical and spectroscopic analyses carried out in organic and aqueous media reveal that formation of intramolecular π-dimers requires the presence of cucurbit[8]uril acting as an assembling element. Evidences for intermolecular dimerization came from electrochemistry data, supporting the existence of chemical steps coupled to the electron transfer processes, and from UV-Vis spectroscopy data collected after exhaustive chemical or photochemical reduction of the samples, with the observation of diagnostic absorption bands, most notably in the near infra-red region. All our conclusions were supported by computational investigations which provided key insights into the structure of the self-assembled intramolecular π-dimers and into the conformation of the discrete pseudo-rotaxane like caviplexes. The CB[8] hosts not only proved useful to promote the redox-triggered formation of supramolecular assemblies in solution, it was also found to prevent the chemical reduction of the porphyrin ring in aqueous media and its subsequent conversion into phlorin products.

Acknowledgments

The authors thank the joint AUCANI (Universidade de São Paulo)-UdL (Université de Lyon) Seed Funding and by the COFECUB program (COFECUB Uc Ph-C 168-17) as well as the Universidade de São Paulo and the Ecole Normale Supérieure de Lyon (ENSL) for financial, logistical and administrative supports. FAPESP (2016/12666-1) and CNPq (309570/2015-8) are also aknowledged. This work was supported by the "Agence National de la Recherche" (ANR-12-BS07-0014-01) and the LABEX iMUST (ANR-10-LABX-0064) of Universit8 de Lyon, within the program "Investissements d'Avenir" (ANR-11-IDEX-0007).

References

[1] E. Krieg, M.M.C. Bastings, P. Besenius, B. Rybtchinski, Supramolecular Polymers in Aqueous Media, Chemical reviews, 116 (2016) 2414.
[2] X.-Y. Hu, T. Xiao, C. Lin, F. Huang, L. Wang, Dynamic Supramolecular Complexes Constructed by Orthogonal Self-Assembly, Accounts of Chemical Research, 47 (2014) 2041−2051.
[3] L. Yang, X. Tan, Z. Wang, X. Zhang, Supramolecular Polymers: Historical Development, Preparation, Characterization, and Functions, Chemical reviews, 115 (2015) 7196.
[4] M.W. Hosseini, Molecular Tectonics: From Simple Tectons to Complex Molecular Networks, Accounts of Chemical Research, 38 (2005) 313.
[5] J.-M. Lehn, From supramolecular chemistry towards constitutional dynamic chemistry and adaptive chemistry, Chemical Society Reviews, 36 (2007) 151.
[6] A. Wang, W. Shi, J. Huang, Y. Yan, Adaptive soft molecular self-assemblies, Soft Matter, 12 (2016) 337.
[7] S. Rieth, C. Baddeley, J.D. Badjic Prospects in controlling morphology, dynamics and responsiveness of supramolecular polymers, Soft Matter, 3 (2007) 137.
[8] L.R. Hart, J.L. Harries, B.W. Greenland, H.M. Colquhoun, W. Hayes, Healable supramolecular polymers, Polymer Chemistry, 4, (2013) 4860.
[9] A.J. McConnell, C.S. Wood, P.P. Neelakandan, J.R. Nitschke, Stimuli-Responsive Metal−Ligand Assemblies, Chemical Review, 115 (2015) 7729−7793.
[10] C. Kahlfuss, S. Denis-Quanquin, N. Calin, E. Dumont, M. Garavelli, G. Royal, S. Cobo, E. Saint-Aman, C. Bucher, Electron-Triggered Metamorphism in Porphyrin-Based Self-Assembled Coordination Polymers, Journal of the American Chemical Society, 138 (2016) 15234.
[11] C. Kahlfuss, T. Gibaud, S. Denis-Quanquin, S. Chowdhury, G. Royal, F. Chevallier, E. Saint-Aman, C. Bucher, Redox-Induced Molecular Metamorphism Promoting a Sol/Gel Phase Transition in a Viologen-Based Coordination Polymer, Chemistry a European Journal, 24 (2018) 13009.
[12] C. Kahlfuss, R. Gruber, E. Dumont, G. Royal, F. Chevallier, E. Saint-Aman, C. Bucher, Dynamic Molecular Metamorphism involving Palladium-Assisted Dimerization of π-Cation Radicals, Chemistry - A European Journal, Just accepted (2018).
[13] C. Kahlfuss, E. Métay, M.-C. Duclos, M. Lemaire, A. Milet, E. Saint-Aman, C. Bucher, Chemically and Electrochemically Triggered Assembly of Viologen Radicals: Towards Multi-addressable Molecular Switches, Chemistry a European Journal, 21 (2015) 2090.

[14] C. Kahlfuss, E. Métay, M.-C. Duclos, M. Lemaire, M. Oltean, A. Milet, E. Saint-Aman, C. Bucher, Reversible Dimerization of Viologen Radicals Covalently Linked to a Calixarene Platform: Experimental and Theoretical Aspects, Compte Rendus Chimie, 17 (2014) 505.
[15] C. Kahlfuss, A. Milet, J. Wytko, J. Weiss, E. Saint-Aman, C. Bucher, Hydrogen-Bond Controlled π-Dimerization in Viologen-Appended Calixarenes: Revealing a Subtle Balance of Weak Interactions, Organic Letters, 17 (2015) 4058.
[16] C. Kahlfuss, E. Saint-Aman, C. Bucher, Redox-controlled intramolecular motions triggered by π-dimerization and πmerization processes, in: T. Nishinaga (Ed.) Organic Redox Systems: Synthesis, Properties, and Applications, John Wiley and sons, New-York, 2016, pp. 39.
[17] A. Iordache, R. Kanappan, E. Métay, M.-C. Duclos, S. Pellet-Rostaing, M. Lemaire, A. Milet, E. Saint-Aman, C. Bucher, Redox Control of Molecular Motions in Bipyridinium Appended Calixarenes, Organic and Biomolecular Chemistry, 11 (2013) 4383.
[18] A. Iordache, M. Oltean, A. Milet, F. Thomas, B. Baptiste, E. Saint-Aman, C. Bucher, Redox control of rotary motions in ferrocene-based elemental ball bearings, Journal of the American Chemical Society, 134 (2012) 2653.
[19] A. Iordache, M. Retegan, F. Thomas, G. Royal, E. Saint-Aman, C. Bucher, Redox Responsive Porphyrin-based Molecular Tweezers, Chemistry a European Journal, 18 (2012) 7648.
[20] R. Kannappan, C. Bucher, E. Saint-Aman, G. Royal, J.-C. Moutet, A. Milet, M. Oltean, E. Métay, S. Pellet-Rostaing, M. Lemaire, C. Chaix, Viologen based redox switchable anion binding receptors, New Journal of Chemistry, 34 (2010) 1373.
[21] D.-W. Zhang, J. Tian, L. Chen, L. Zhang, Z.-T. Li, Dimerization of Conjugated Radical Cations: An Emerging Non- Covalent Interaction for Self-Assembly, Chemistry an Asian Journal, 10 (2015) 56.
[22] J.M. Spruell, Molecular recognition and switching via radical dimerization, Pure & Applied Chemistry, 82 (2010) 2281.
[23] J.-M. Lu, S.V. Rosokha, J.K. Kochi, Stable (Long-Bonded) Dimers via the Quantitative Self-Association of Different Cationic, Anionic, and Uncharged ð-Radicals: Structures, Energetics, and Optical Transitions, Journal of the American Chemical Society, 125 (2003) 12161.
[24] T. Nishinaga, K. Komatsu, Persistent π radical cations: self-association and its steric control in the condensed phase, Organic & Biomolecular Chemistry, 3 (2005) 561.
[25] M. Kertesz, Pancake Bonding: An Unusual Pi-Stacking Interaction, Chemistry – A European Journal, 25 (2019) 400.
[26] M.R. Geraskina, A.S. Dutton, M.J. Juetten, S.A. Wood, A.H. Winter, The viologen cation radical pimer: a case of dispersion-driven bonding, Angewandte Chemie, International Edition in English, 129 (2017) 9563.
[27] P.M.S. Monk, N.M. Hodgkinson, S.A. Ramzan, Spin pairing ('dimerisation') of the viologen radical cation: kinetics and equilibria, Dyes and Pigments, 43 (1999) 207.
[28] M. Berville, L. Karmazin, J.A. Wytko, J. Weiss, Viologen cyclophanes: redox controlled host–guest interactions, Chemical Communications, 51 (2015) 15772.
[29] M. Berville, S. Choua, C. Gourlaouen, C. Boudon, L. Ruhlmann, C. Bailly, S. Cobo, E. Saint-Aman, J. Wytko, J. Weiss, Flexible Viologen Cyclophanes: Odd/Even Effects on Intramolecular Interactions, ChemPhysChem, 18 (2017) 796.
[30] H.D. Correia, S. Chowdhury, A.P. Ramos, L. Guy, G.J.-F. Demets, C. Bucher, Dynamic Supramolecular Polymers Built From Cucurbit[n]urils And Viologens, Polymer International, (2018) Accepted Manuscript.

[31] K. Madasamy, V.M. Shanmugam, D. Velayutham, M. Kathiresan, Reversible 2D Supramolecular Organic Frameworks encompassing Viologen Cation Radicals and CB[8], Scientific Reports, 8 (2018) 1354.
[32] E. Pazos, P. Novo, C. Peinador, A.E. Kaifer, M.D. García, Cucurbit[8]uril (CB[8])-Based Supramolecular Switches, Angewandte Chemie International Edition, 58 (2019) 403.
[33] L. Isaacs, Stimuli Responsive Systems Constructed Using Cucurbit[n]uril-Type Molecular Containers, Accounts of Chemical Research, 47 (2014) 2052−2062.
[34] E. Masson, X. Ling, R. Joseph, L. Kyeremeh-Mensah, X. Lu, Cucurbituril chemistry: a tale of supramolecular success, RSC Advances, 2 (2012) 1213.
[35] H. Zou, J. Liu, Y. Li, X. Li, X. Wang, Cucurbit[8]uril-Based Polymers and Polymer Materials, Small, 14 (2018) 1802234.
[36] Z. Han, Q. Zhou, Y. Li, Self-assembled (pseudo)rotaxane and polyrotaxane through host–guest chemistry based on the cucurbituril family, Journal of Inclusion Phenomena and Macrocyclic Chemistry, 92 (2018) 81.
[37] H. Yin, R. Rosas, D. Gigmes, O. Ouari, R. Wang, A. Kermagoret, D. Bardelang, Metal Actuated Ring Translocation Switches in Water, Organic Letters, 20 (2018) 3187.
[38] Y.H. Ko, E. Kim, I. Hwang, K. Kim, Supramolecular assemblies built with host-stabilized charge-transfer interactions, Chemical Communications, (2007) 1305.
[39] J. Liu, C.S.Y. Tan, Y. Lan, O.A. Scherman, Aqueous Polymer Self-Assembly Based on Cucurbit[n]uril-Mediated Host-Guest Interactions, Macromolecular Chemistry and Physics, 217 (2016) 319.
[40] X. Zhang, C.-B. Nie, T.-Y. Zhou, Q.-Y. Qi, J. Fu, X.-Z. Wang, L. Dai, Y. Chen, X. Zhao, The construction of single-layer two-dimensional supramolecular organic frameworks in water through the self-assembly of rigid vertexes and flexible edges, Polymer Chemistry, 6 (2015) 1923.
[41] W.-C. Cheng, M.J. Kurth, The Zincke reaction. A review, Organic Preparations and Procedures International, 34 (2002) 585.
[42] V.-A. Constantin, L. Cao, S. Sadaf, L. Walder, Oligo-viologen/SWCNT nano-composites: Preparation and characterization, physica status solidi (b), 249 (2012) 2395.
[43] D. Bardelang, K.A. Udachin, D.M. Leek, J.A. Ripmeester, Highly symmetric columnar channels in metal-free cucurbit[n]uril hydrate crystals (n = 6, 8), CrystEngComm, 9 (2007) 973.
[44] J. Lagona, P. Mukhopadhyay, S. Chakrabarti, L. Isaacs, The Cucurbit[n]uril Family, Angewandte Chemie, International Edition in English, 44 (2005) 4844.
[45] E. Masson, M. Raeisi, K. Kotturi, Kinetics Inside, Outside and Through Cucurbiturils, Israel Journal of Chemistry, 58 (2018) 413.
[46] F. Ammar, J.-M. Savéant, Convolution Potential Sweep Voltammetry. II. Multistep Nernstian waves Journal of Electroanalytical Chemistry, 47 (1973) 215.
[47] F. Ammar, J.M. Saveant, Thermodynamics of successive electron transfers. Internal and solvation enthalpy and entropy variations in a series of polynitrocompounds. , Journal of Electroanalytical Chemistry and Interfacial Electrochemistry, 47 (1973) 115.
[48] K.M. Kadish, L.R. Shiue, R.K. Rhodes, L.A. Bottomley, Reactions of Metalloporphyrin p Radicals. 1. Complexation of Zinc Tetraphenylporphyrin Cation and Anion Radicals with Nitrogenous Bases, Journal of the American Chemical Society, 20 (1981) 1274.
[49] E. Van Caemelbecke, A. Derbin, P. Hambright, R. Garcia, A. Doukkali, A. Saoiabi, K. Ohkubo, S. Fukuzumi, K.M. Kadish, Electrochemistry of [(TMpyP)MII]4+(X-)4 (X- = Cl- or BPh4-) and [(TMpyP)MIIICl]4+(Cl-)4 in N,N-Dimethylformamide Where M Is One of 15 Different Metal Ions, Inorganic Chemistry, 44 (2005) 3789.
[50] S. Baral, P. Hambright, P. Neta, One- and two-electron reduction of aluminum and tin pyridylporphyrins. A kinetic spectrophotometric study, The Journal of Physical Chemistry, 88 (1984) 1595.

[51] M.C. Richoux, P. Neta, A. Harriman, S. Baral, P. Hambright, One- and two-electron reduction of metalloporphyrins. Radiation chemical, photochemical, and electrochemical studies. Kinetics of the decay of .pi.-radical anions, The Journal of Physical Chemistry, 90 (1986) 2462.
[52] K. Kalyanasundaram, M. Neumann-Spallart, Photophysical and redox properties of water-soluble porphyrins in aqueous media, The Journal of Physical Chemistry, 86 (1982) 5163.
[53] W. Sliwa, T. Zujewska, M. Mielniczak, Porphyrins bearing quaternary pyridinium substituents, Chemistry of Heterocyclic Compounds, 29 (1993) 617.
[54] K.M. Kadish, C. Araullo, G.B. Maiya, D. Sazou, J.M. Barbe, R. Guilard, Electrochemical and spectral characterization of copper, zinc, and vanadyl meso-tetrakis(1-methylpyridinium-4-yl)porphyrin complexes in dimethylformamide, Inorganic Chemistry, 28 (1989) 2528.
[55] W.S. Jeon, E. Kim, Y. Ho Ko, I. Hwang, J.W. Lee, S.-Y. Kim, H.-J. Kim, K. Kim, Molecular loop lock: A redox-driven molecular machine based on a host-stabilized charge-transfer complex, Angewandte Chemie International Edition in English, 44 (2005) 87
[56] W.S. Jeon, H.J. Kim, C. Lee, K. Kim, Control of the stoichiometry in host-guest complexation by redox chemistry of guests: inclusion of methylviologen in cucurbit[8]uril, Chemical Communications, (2002) 1828.
[57] W.S. Jeon, A.Y. Ziganshina, J.W. Lee, Y.H. Ko, J.-K. Kang, C. Lee, K. Kim, A [2]Pseudorotaxane-Based Molecular Machine:Reversible Formation of aMolecular Loop Driven by Electrochemical and Photochemical Stimuli, Angewandte Chemie International Edition in English, 42 (2003) 4097.
[58] H.-J. Kim, W.S. Jeon, Y.H. Ko, K. Kim, Inclusion of methylviologen in cucurbit[7]uril, Proceedings of the National Academy of Sciences, 99 (2002) 5007.
[59] S.G. Mayhew, The redox potential of dithionite and SO_2^- from equilibrium reactions with flavodoxins, methyl viologen and hydrogen plus hydrogenase, European Journal of Biochemistry, 85 (1978) 535.
[60] P. Neta, One-electron transfer reactions involving zinc and cobalt porphyrins in aqueous solutions, The Journal of Physical Chemistry, 85 (1981) 3678.
[61] K. Kalyanasundaram, Mechanism of photoreduction of water-soluble palladium and zinc porphyrins, Journal of Photochemistry and Photobiology A: Chemistry, 42 (1988) 87.
[62] S. Baral, P. Neta, P. Hambright, Spectrophotometric and kinetic studies of the radiolytic reduction of several pyridylporphyrins and their metal complexes, Radiation Physics and Chemistry (1977), 24 (1984) 245.
[63] A. Harriman, Metalloporphyrin-photosensitized formation of hydrogen from organic and inorganic substrates, Journal of Photochemistry, 29 (1985) 139.
[64] R. Bonnet, R.J. Ridge, E.J. Land, R.S. Sinclair, D. Tait, T.G. Truscott, Pulsed irradiation of water-soluble porphyrins, Journal of the Chemical Society, Faraday Transactions 1: Physical Chemistry in Condensed Phases, 78 (1982) 127.
[65] Y. Harel, D. Meyerstein, Mechanism of reduction of porphyrins. Pulse radiolytic study, Journal of the American Chemical Society, 96 (1974) 2720.
[66] A. Harriman, M.C. Richoux, P. Neta, Redox chemistry of metalloporphyrins in aqueous solution, The Journal of Physical Chemistry, 87 (1983) 4957.
[67] Z.M. Abou-Gamra, N.M. Guindy, Photochemistry of metalloporphyrins in aqueous solutions, Spectrochimica Acta Part A: Molecular Spectroscopy, 45 (1989) 1207.
[68] Y. Fang, Y.G. Gorbunova, P. Chen, X. Jiang, M. Manowong, A.A. Sinelshchikova, Y.Y. Enakieva, A.G. Martynov, A.Y. Tsivadze, A. Bessmertnykh-Lemeune, C. Stern, R. Guilard, K.M. Kadish, Electrochemical and Spectroelectrochemical Studies of Diphosphorylated Metalloporphyrins. Generation of a Phlorin Anion Product, Inorganic Chemistry, 54 (2015) 3501.

[69] M. Ishida, K. Nakahara, R. Sakashita, T. Ishizuka, M. Watanabe, H. Uno, A. Osuka, H. Furuta, N-confused phlorin: a stable dihydroporphyrin isomer containing a confused pyrrole ring, Journal of Porphyrins and Phthalocyanines, 18 (2014) 909.
[70] G.S. Wilson, G. Peychal-Heiling, Electrochemical studies of some porphyrin IX derivatives in aprotic media, Analytical Chemistry, 43 (1971) 545.
[71] J.G. Lanese, G.S. Wilson, Electrochemical Studies of Zinc Tetraphenylporphin, Journal of the Electrochemical Society, 119 (1972) 1039.
[72] M. Mahesh, J.A. Murphy, F. LeStrat, H.P. Wessel, Reduction of arenediazonium salts by tetrakis(dimethylamino)ethylene (TDAE): Efficient formation of products derived from aryl radicals, Beilstein Journal of Organic Chemistry, 5 (2009) 1.
[73] W.S. Abdul-Hassan, D. Roux, C. Bucher, S. Cobo, F. Molton, E. Saint-Aman, G. Royal, Redox-Triggered Folding of Self-Assembled Coordination Polymers incorporating Viologen Units, Chemistry - A European Journal, 24 (2018) 12961.
[74] T. Nagamura, N. Takeyama, T. Matsuo, Cooperative sensitization in photoreduction of viologens by metals complexes and charge-transfer complexes on amphipathic viologen micelles, Chemistry Letters, (1983) 1341.
[75] Y. Zhao, D.G. Truhlar, The M06 suite of density functionals for main group thermochemistry, thermochemical kinetics, noncovalent interactions, excited states, and transition elements: two new functionals and systematic testing of four M06-class functionals and 12 other functionals, Theoretical Chemistry Accounts, 120 (2008) 215.
[76] M. Capdevila-Cortada, J. Ribas-Arino, J.J. Novoa, Assessing the performance of CASPT2 and DFT methods for the description of long, multicenter bonding in dimers between radical ions, Journal of Chemical Theory and Computation, 10 (2014) 650.